An Investigation of Three Supersonic Wings at Mach 2, 3 and 5 using Computational Fluid Dynamics

Daire O'Sullivan

20249748

Supervisor: Dr. Philip Griffin

Second Reader: Vanessa Egan

Bachelor of Engineering Final Year Project report submitted to the University of Limerick, April 2024 for the award:

Bachelor of Engineering (BE) in Aeronautical Engineering

School of Engineering

Declaration

I declare that this is my work and that all contributions from other persons have been appropriately identified and acknowledged.

Sign Name: 

Print Name DÁIRE O'SULLIVAN

Acknowledgments

I would like to thank my supervisor Professor Philip Griffin for his support and guidance throughout this project. Without his initial and continuous encouragement this report would not exist.

I would also like to thank my friends and family for their support throughout this project and the years of study that preceded it.

Contents

Acknowledgments i

Contents i

Abstract ii

Nomenclature iii

Introduction 1

1.1 Project Background 1

1.2 Project Objectives 2

2 Literature Review 2

2.1 Supersonic Aerodynamics 2

2.2 Supersonic Computational Fluid Dynamics 6

3 Review of Theory 7

3.1 Shockwaves 7

3.2 Prandtl-Meyer Expansion Waves 9

3.3 Linear Theory 10

3.4 Computational Fluid Dynamics 10

4 Wing Geometry 12

4.1 Biconvex Wing 12

4.2 Round LE Delta Wing 13

4.3 Wedge Delta Wing 13

5 Methodology 14

5.1 Geometry Setup 14

5.2 Boundary Setup 14

5.3 Physics and Initial Conditions 15

5.4 Solvers 15
5.5 Overset Setup 16
5.6 Mesh Independence Study and Simulation Validation 16
6 Meshing 18
6.1 Part 1 18
6.2 Part 2 20
7 Zero-Lift Results 20
7.1 Shockwave Geometry 20
7.2 Simulation and Theoretical Results 22
8 Lifting Performance Results 25
9 Discussion 26
10 Conclusion and Future work 27
A. Biconvex Wing Section 1
B. Wedge Delta Wing Section 2
C. Round LE Delta Wing Section 3
D. Wing Renders 4
E. Volume Rendering on Round LE Delta Wing at Mach 2 4
F. Section Showing Conical Flow on Wedge Delta Wing at Mach2 6
G Pressure and Mach Distribution on Wing Surface 7
H Root Section of Wings 10
I Section at 1m of Span of Wings 10
J Results of CFD and Oblique Shock Theory 11
K Shock Expansion Theory MATLAB Code 14
L Linear Theory MATLAB Code 15

Abstract

This report seeks to assess the accuracy of the STARCCM+ CFD software in simulating the supersonic flow over wings. Supersonic flows have many applications in the aerospace industry. Special attention will be given to the formation of shockwaves and the effect wing geometry and Mach number has on their development. Secondary to this will be the assessment of the performance characteristics of different supersonic wings. Investigations were performed on three wing geometries representative of that commonly found in supersonic studies.StarCCM+ has been used to simulate the flow over three wing geometries

at Mach 2, 3 and 5. An Adaptive Mesh Refinement Solver was used to reduce the computational load while still retaining enough mesh density to resolve discontinuities within the flow.The results from STARCCM+ have been validated using oblique shock theory and previous wind tunnel experiments as found in the literature. It was found that StarCCM+ produced results that are in strong agreement with both windtunnel testing and theory. The three wings were simulated at varied angles of attack to assess their performance at Mach 2 and it was found that a moderately swept biconvex wing had the greatest value of C_L.

Nomenclature

Symbols	Meaning	Units
$\in$	Wing Vertex Half Angle	Degrees
A	Aspect Ratio	-
AOA	Angle of Attack	Degrees
c	Airfoil chord length	Metres
C_D	Coefficient of Drag	-
C_L	Coefficient of Lift	-
LE	Leading Edge	
M	Mach Number	-
M_N	Mach Number normal to shockwave	-
p	Static Pressure	Pascals
t	Thickness of airfoil	-
α	Angle of Attack	Degrees
β	Angle of Shockwave	Degrees
γ	Ratio of specific heats	
θ	Deflection Angle of Leading Edge	Degrees
Λ	Leading Edge Sweep	Degrees
μ	Mach Angle	Degrees
f	Body force	Newtons
$\dot{q}$	Heat flux	W/m^2
t	time	seconds
ρ	Density	Kg/m^3
x	x-component	-
y	y-component	-
z	z-component	-
u	x-component of velocity	m/s
v	y-component of velocity	m/s
w	z-component of velocity	m/s
e	Specific internal energy	J/kg

Introduction

1.1 Project Background

Interest in expanding supersonic flight beyond military use has been expanding in recent years. NASA are currently developing the X-59 with the hope of quieting the sonic boom of a potential supersonic transport aircraft((NASA 2024). Several companies are actively developing supersonic transport aircraft. One of these companies, Boom Supersonic has recently test flown a prototype(Boom 2024).

Interest in hypersonic flight has also been increasing. Although a lot of this has been motivated by military interest, companies such as Hermeus are developing aircraft such as the Halycon shown in Figure 1-1 as the future of high-speed transport(Hermeus 2024)

Recent developments in reusable launch vehicles have seen an increase in the use of supersonic grid fins. Typically found on missiles, these control surfaces have many advantages over standard control surfaces at supersonic and hypersonic velocities'(Schülein and Guyot 2006). Although they can be configured as straight rectangular fins, more efficient designs have a similar design to a delta wing and can be analysed as such.

Unfortunately, due to the lack of development in supersonic flight in both the commercial and civil aviation industries since the retirement of the Concorde, there is little recent research publicly available.

It upon this backdrop of renewed interest in supersonic flight that this report seeks to assess the suitability of commercial CFD codes for examining these types of flows. In 1947 Theodore von Karman asserted that "knowledge of supersonic aerodynamics should be considered by the aeronautical engineer as a necessary prerequisite to his art"(Karman 1947). This is now true more than ever when the widespread availability of highspeed computers means that supersonic analysis is no longer restricted to large organisations with expensive windtunnels.

Figure 0-1 Hermeus' under development Halcyon hypersonic aircraft (Hermeus 2024).

However, there is also evidence to suggest increased that supersonic transports can have an adverse effect on the environment. Noise pollution and exhaust fumes are of particular concern(Drake and Purvis 2001). Restrictions on supersonic flight limited the success of the Concorde, therefore the issue of supersonic booms must be addressed for widespread uptake of supersonic vehicles.

"Computational Fluid Dynamics (CFD), once the domain of academics, post-doctoral researchers or trained specialists, is now progressively

becoming more accessible to graduate engineers for research and development"(Tu *et al.* 2018). The development of CFD has so far allowed for faster aircraft development times and increased performance(Jameson 2012). CFD can act as a replacement for experimental fluid dynamics e.g. wind tunnel testing at the beginning of a design project. This is especially true for supersonic flow as supersonic wind tunnels are expensive to run and for extremely high Mach numbers can often only run the flow conditions for a split second. The numerical methodology used allows for much more accurate solutions than can be found through analytical means. However, computer resources are still finite and certain approximations must still be made. Therefore, CFD acts as one element in the engineer's design toolbox(Anderson 1995). Predictions of detached and bow-shockwaves can be particularly difficult with analytical methods due to the highly non-linear nature of these flows(Anderson 2003).

1.2 Project Objectives

The intent of this project is to use Computational Fluid Dynamics software to simulate the flow over wings at supersonic velocities. The validity of the software in simulating these flows will be established and contrasted with some of the early theoretical methods. Oblique shock theory and linear theory will be used throughout to validate and compare with the CFD where appropriate.

The report will be split into two parts. In Part 1, the wings will be simulated at their zero-lift condition. Particular attention will be given to the formation of shockwaves on the wing and how the freestream Mach number and the wing geometry affect this.

Part 2 will examine the lifting condition of the wing. The wings will be simulated at a range of AOA using an overset mesh. A steady simulation will then be performed at the value of α for which C_L/C_D is maximum. The effect of the wing geometry on the results will be discussed.

Through this work a supersonic CFD workflow will be established.

2 Literature Review

2.1 Supersonic Aerodynamics

Supersonic flow is defined as flow where the Mach number is greater than 1 everywhere in the flow(Anderson 2003) i.e., the flow is uniformly faster than the speed of sound. At these velocities, disturbances in the flow are unable to propagate ahead and alert the upstream flow. Shockwaves form when this flow is compressed ahead of the disturbance. There are a number of key facts surrounding supersonic flow that can be found in any good text on the subject, below are some of these from (Anderson 2003);

- Shockwaves are thin discontinuities in the flow across which the static temperature, density and temperature increase and the velocity decreases. These changes occur suddenly and non-isentropically.

- Oblique shockwaves occur when flow is turned into itself, as it would be as it meets the leading edge (LE) of a wing at an angle θ. A shockwave will be formed at an angle β that diverts the flow by the angle θ.
- If the values upstream of the shock wave and the deflection angle are known, then the downstream values can be calculated using oblique shock theory.
- Expansion waves are the inverse of a shockwave. A flow is turned away from itself and the values are isentropically varied gradually.
- Across an expansion wave the static temperature, pressure and density decrease while the Mach number increases.
- If the values upstream of the expansion wave and the deflection angle are known, then the downstream values can be calculated using the Prandtl-Meyer function.
- As a disturbance travels through a fluid at M>1, a Mach wave is formed with an angle μ. Figure 3-1 shows this process forming a "Mach cone".

"Flows in which viscosity, thermal conduction, and diffusion are ignored are called *inviscid flows*" (Anderson 2003). Most of the supersonic literature surveyed for this report has treated the flow as inviscid as it is possible to calculate surface distributions accurately with this assumption.

Hypersonic flow is usually classified as flow where M>5 although there is no observable difference in the flow condition at this velocity. Rather, hypersonic flow is best classified as the point at which certain phenomena begin to occur. These include severe heating, combustion, thick boundary layers and non-linearities within the flow. These effects make hypersonic flow distinct enough from supersonic flow that new methods are required for studying it(Anderson 2003). At hypersonic speed the value of beta can become extremely small and boundary layer interaction with the shockwave can become significant enough that the flow can no longer be considered inviscid. Hypersonic effects have been included briefly as simulations at Mach 5 might display some of these effects.

Even firmly within the supersonic regime, the properties of air can change. For flow below Mach 3, air is generally treated as calorically perfect and γ=1.4 (Anderson 2003). However, at value above Mach 3, the air is considered to be thermally perfect and a polynomial or table of values is needed for γ(Siemens 2022).

Although both subsonic and supersonic wings rely on a pressure differential across the bottom and top surfaces to create lift, the manner in which this differential is achieved is quite different. Supersonic airfoils tend to be symmetrical to reduce the wave drag. Therefore, it is necessary for the wing to be at an angle of attack for any lift to be produced. Supersonic wings and airfoils rely on the changes in pressure downstream of a shock or an expansion wave to create the pressure difference. On a supersonic airfoil the majority of this positive pressure is generated by the lower surface(Bertin and Cummings 2014). This in contrast to a subsonic airfoil in which the majority of the positive pressure is generated by the upper surface.

The basic facts of supersonic flow are based on theoretical and experimental research that dates back to the 1920's. The governing equations of supersonic flow are non-linear in nature(Vincenti 1951). To begin approaching the calculation of forces on an airfoil early researchers found it necessary to make some assumptions in order to simplify the problem.

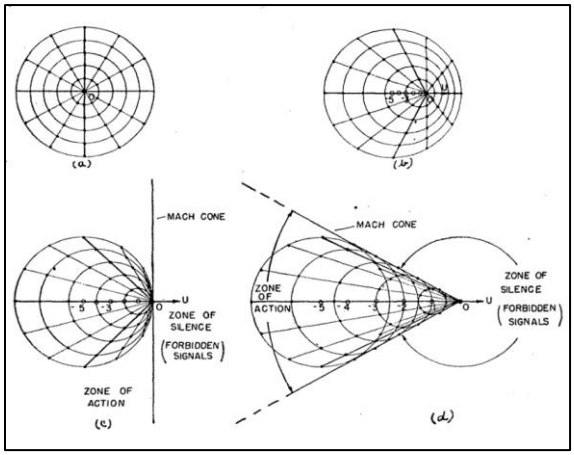

Figure 2-1 Propagation of disturbances in supersonic flow (Karman 1947)

Firstly, that due to the supersonic velocity, for a thin airfoil with a sharp leading edge, any disturbances are kept within the Mach Cone (Ackeret 1925). The LE can then be said to make a small disturbance to the flow. Treating these disturbances as Mach waves instead of a pressure wave the flow is isentropic(Bertin and Cummings 2014) it is then possible to calculate the pressure change across the surface of the airfoil using Prandtl-Meyer relations. Using these assumptions leads to an equation for C_L that is dependent on α and M only. Drag however is dependent on the camber and thickness of the airfoil(Bertin and Cummings 2014). These equations are known together as linear theory. Interestingly, (Anderson 2003) does not mention a term for drag due to lift while it is included in (Bertin and Cummings 2014) description of linear theory. Also included in (Bertin and Cummings 2014) is a viscous drag correction term which is also present in (Ulmann and Bertram 1953). This correction term is used to bring values of drag in line with wind tunnel testing.

A more accurate estimation of the pressures on the surface of the airfoil can be made using "Shock-Expansion Theory". This is the name used for the direct calculation of wing surface pressure using Oblique Shock theory and the Prandtl-Meyer function(Vincenti 1951). Although this method yields better results it can be extremely time consuming.

Both shock expansion and linear theory are two-dimensional theories, however sections of the wing that fall outside the Mach cone can be treated as two-dimensional(Vincenti 1951).

The theories examined so far have assumed an infinite straight wing in supersonic flow. (Jones 1945) suggests that by sweeping the wing, much greater performance can be achieved due to the fact that only the component of the flow perpendicular to the wings leading edge contributes to the pressure on the wing. For aircraft operating in the transonic regimes, this can delay the onset of critical drag. For supersonic wings, if the wing is swept behind the Mach cone, the wing can be treated as subsonic. This phenomenon is shown in Figure 3-2.

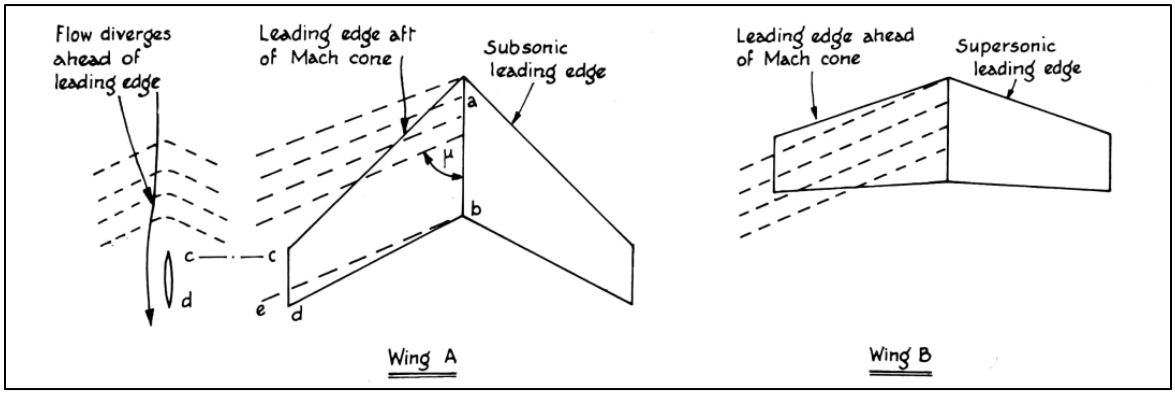

Figure 2-2 Whitford 1989

(Love 1949) conducted tests on 11 different triangular planforms with sharp and rounded leading edges. These experiments were specifically conducted to compare experimental data with the linear theory. A leading-edge parameter $\frac{\tan \epsilon}{\tan m}$, also known as a tangent ratio is established and is used to correlate the sweep of the wing with the angle of the Mach cone where a value of 1 means that the angles are equal. Also examined was the effect of a rounded leading edge on the performance of the wings. He finds that for wings with their leading edge coincident with the Mach cone that they do not agree well with theory. For values of $\frac{\tan \epsilon}{\tan m}$ below 1, ie the wing is swept behind the Mach Cone, linear theory was in poor agreement with the experimental results. However, for wings with leading edges far ahead of the Mach cone, experimental values were in very good agreement with the linear theory. It was also found that these wings had higher lift curves also. This result would seem to contradict the work of Jones (1945) who suggests that advanced sweepback can avoid critical drag. Love (1949) also found that elliptical LE did not create any kind of suction that might reduce drag. Fortunately, this report included Schlieren images of the experiments which can be used to compare with the results of the CFD experiments.

(Vincenti 1951) also makes a direct comparison between wind tunnel testing and theoretical results. He notes that large disturbances can form which destroy the assumption of a Mach cone confining all disturbances. He finds that increased sweep towards the Mach cone first results in an increase in drag followed by a reduction. This is in agreement with (Love 1949). In his report Vincenti finds an 8-10% lower lift on the experimentally tested wings as compared to the linear theory.

(Ulmann and Bertram 1953) also present a comparison between the linear theory and wind tunnel testing being undertaken across NACA in the early 50's. In this paper wind tunnel data for wings having double-wedge airfoil sections is compared with linear theory for Mach Numbers of 4.04 and 6.9. They find that the experimental data diverges from the linear theory for angles of attacks above 6 ° and wings with thick leading edges. For the higher Mach numbers, they establish that the linear theory is not suitable. They find that shock-expansion theory and the method of characteristics had better correlation with the experimental data. These more developed theories take into account the actual geometry of the wing and the possibility for shock detachment.

(Wood 1988) summarises the previous work completed and also introduces some results of non-linear theory. This report serves as a retrospective of previous work in the area with the benefit of the context of early CFD. He notes the inability of linear theory to correlate with experimental results. He introduces a new term βcot Λ which is equivalent to $\frac{\tan \epsilon}{\tan m}$. He explains that for values of βcot Λ>0.5 that the non-linear and linear theory diverges. This is in agreement with some of (Love 1949) which found that for values of $\frac{\tan \epsilon}{\tan m}$ between 0.5 an 0.6 experimental values were much less than the linear theory. This suggests the accuracy of non-linear techniques.

2.2 Supersonic Computational Fluid Dynamics

Supersonic aerodynamic calculations completed using computers have existed since the 1960's. (Barrowman 1966) details the creation of a Fortran code for calculating the supersonic performance of sounding rocket fins. This program is worth highlighting as it makes use of the computer to solve the exact numerical aerodynamic equations. This is contrast to the simplifications needed to derive the analytical solutions described above.

Computational Fluid Dynamics is a catch-all term for a number of mathematical techniques that take advantage of modern computing to compliment traditional fluid dynamics techniques. (Anderson 1995) provides a good introduction into the theory and philosophy of Computational Fluid Dynamics. Although much of the application been out-dated, much of the fundamentals here are still valid.

The accurate simulation of supersonic flows requires the use of fine meshes and higher order discretisation schemes.(Zore *et al.* 2020) utilised an unstructured 'HexTet' mesh flow to capture the shockwaves on an "Axie" shape in an inviscid Mach 1.6 flow. A mesh adaptation function is used to refine the mesh to 198 million elements. They found that the results of their simulation were in close agreement with those found in the AIAA Supersonic Boom Prediction Workshops. Notably, they find that a cell element count of 49 million was insufficient to resolve the flow.

(Cross and West 2019) utilised an Adaptive Mesh refinement to reduce the density of their overall mesh while providing sufficient density at where shockwaves form. This report is

particularly relevant as the authors use StarCCM+. However, they are simulating at Mach 6 and beyond, which is where they note oxygen begins to dissociate. Nevertheless, good insight is given into the high-speed compressible flow solvers available in StarCCM+ and the best practices to follow when using these.

3 Review of Theory

3.1 Shockwaves

As the velocity of an object in flight is increased into the supersonic region, shockwaves and their effects on the flow dominate all aspects of aerodynamics(Anderson 2003). On sharp objects such as the Biconvex and Wedge Delta wings examined in this report the shockwave will be attached and oblique.

As this disturbance moves through the flow a Mach Angle unique to the Mach number of the object can be found.

$$\mu = sin^{-1}\frac{1}{M} \tag{1}$$

The overall geometry of a shockwave will be given by both the velocity of the flow and the shape of the object moving through the flow. The angle at which this shockwave forms can be calculated using the β-θ-M relationship where θ is the angle of deflection of the LE, M is the Mach number and β is the angle of the shock wave. This equation is presented as follows in (Anderson 2003):

$$\tan\theta = 2\cot\beta\left[\frac{M_1^2\sin^2\beta - 1}{M_1^2(\gamma + \cos 2\beta) + 2}\right] \tag{2}$$

A more practically useful version can be expressed as the θ-β-M relationship.

$$\tan\beta = \frac{M^2 - 1 = +2\lambda\cos[\frac{4\pi\delta + \cos^{-1}\chi}{3}]}{3(1 + \frac{\gamma - 1}{2}M^2)\tan\theta} \tag{3}$$

Where,

$$\lambda = \left[(M^2-1)^2 - 3\left(1 + \frac{\gamma-1}{2}M^2\right)\left(1 + \frac{\gamma+1}{2}M^2\right)\tan^2\theta\right]^{1/2} \tag{4}$$

$$\chi = \frac{(M^2-1)^3 - 9\left(1+\frac{\gamma-1}{2}M^2\right)\left(1+\frac{\gamma-1}{2}M^2+\frac{\gamma+1}{4}M^4\right)\tan^2\theta}{\lambda^3}$$

(5)

For a given Mach number there exists a value of θ past which the shock wave will become detached from the leading edge.

Given the flow conditions ahead of a shock, the oblique shock relations can be used to calculate the static temperature, velocity and pressure of the flow after passing through a shockwave.

(Anderson 2003) develops the following formulas:

$$M_{n_1} = M_1 \sin\beta$$

(6)

$$\frac{\rho_2}{\rho_1} = \frac{(\gamma+1)M_{n_1}^2}{(\gamma-1)M_{n_1}^2+2}$$

(7)

$$\frac{p_1}{p_2} = 1 + \frac{2\gamma}{\gamma+1}\left(M_{n_1}^2-1\right)$$

(8)

$$M_{n_2}^2 = \frac{M_{n_1}^2 + \left[\frac{2}{\gamma-1}\right]}{\left[\frac{2\gamma}{\gamma-1}\right]M_{n_1}^2 - 1}$$

(9)

$$\frac{T_2}{T_1} = \frac{p_2}{p_1}\frac{\rho_1}{\rho_2}$$

(10)

$$M_2 = \frac{M_{n_2}}{\sin(\beta - \theta)}$$

(11)

3.2 Prandtl-Meyer Expansion Waves

When supersonic flow travels over a convex corner or is "turned away from itself" an expansion wave is formed. In contrast to a shockwave the change of flow properties across an expansion wave is smooth(Anderson 2003). The change of flow conditions is also the inverse of the shockwave as the Mach number increase while the temperature, pressure and density decrease(Anderson 2003).

The following equations can be used to calculate the flow properties across an expansion wave.

$$\nu(M) = \sqrt{\frac{\gamma+1}{\gamma-1}}\tan^{-1}\sqrt{\frac{\gamma-1}{\gamma+1}(M^2-1)} - tan^{-1}\sqrt{M^2-1}$$

(12)

$$\theta_2 = \nu(M_2) - \nu(M_1)$$

(13)

$$\frac{T_1}{T_2} = \frac{1 + \frac{\gamma-1}{2}M_2^2}{1 + \frac{\gamma-1}{2}M_1^2}$$

(14)

$$\frac{p_1}{p_2} = \left[\frac{1 + \frac{\gamma-1}{2}M_2^2}{1 + \frac{\gamma-1}{2}M_1^2}\right]^{\frac{\gamma}{\gamma-1}}$$

(15)

Where θ_2 is the angle of deflection through which the flow has been diverted. If this value along with that of M_1 is known, then the value of M_2 can be found through the iteration using formula X.

The symbol ν represents the Prandtl-Meyer function which takes M as an input.

3.3 Linear Theory

The following formulas will be used in the application of the Linear Theory(Houghton *et al.* 2013).

$$C_L = \frac{4\alpha}{\sqrt{M^2 - 1}} \tag{16}$$

For a double wedge airfoil, the drag can be calculated as follows:

$$c_D = \frac{4}{\sqrt{M^2 - 1}}\left[\alpha^2 + \left(\frac{t}{c}\right)^2\right] \tag{17}$$

For a biconvex airfoil the drag can be calculated as follows:

$$c_D = \frac{4}{\sqrt{M^2 - 1}}\left[\alpha^2 + \frac{4}{3}\left(\frac{t}{c}\right)^2\right] \tag{18}$$

3.4 Computational Fluid Dynamics

The typical method by which a CFD code solves the flow simulation is using the Navier Stokes (NS) equations. CFD codes typically discretise the full equations, this is completed through the use of the mesh that subdivide the flow domain. The NS equations are then solved at the centroid of each cell. There are different methods of discretizing the flow, the two most prominent being the finite element and finite volume method. In the finite volume method which StarCCM+ utilises, the flow is represented as a fixed control volume V in space (Anderson 1995).Within this space the governing equations are applied.

For inviscid flow, the Euler Equations can be utilised instead of the NS equations. This results in huge computational saving as viscous effects are not solved(Siemens 2022). The Euler equations are derived by simply removing all friction and thermal conduction terms from the NS equations (Anderson 1995).

Continuity Equation

$$\frac{\partial \rho}{\partial t} + \nabla \cdot (\rho v) = 0 \tag{19}$$

Momentum Equations

x component

$$\frac{\partial(\rho_U)}{\partial t} + \nabla \cdot (\rho u V) = -\frac{\partial p}{\partial x} + \rho f x \tag{20}$$

y component

$$\frac{\partial(\rho_v)}{\partial t} + \nabla \cdot (\rho u V) = -\frac{\partial p}{\partial y} + \rho f y \tag{21}$$

z component

$$\frac{\partial(\rho_w)}{\partial t} + \nabla \cdot (\rho u V) = -\frac{\partial p}{\partial z} + \rho f z \tag{22}$$

Energy Equation

$$\frac{\partial}{\partial t}\left[\rho\left(e + \frac{V^2}{2}\right)\right] + \nabla \cdot \left[\rho\left(e + \frac{V^2}{2}\right)V\right] = \rho\dot{q} - \frac{\partial(up)}{\partial x} - \frac{\partial(vp)}{\partial y} - \frac{\partial(p)}{\partial z} + \rho f \cdot V \tag{23}$$

4 Wing Geometry

The wing geometries used in this report were taken from existing literature, some of which has been explored in the literature review. This has meant that the wings are realistic and in the case of the Wedge Delta and Round LE Delta, results from wind tunnel testing are available. Delta planforms have been selected for two of the geometries. This is due to their common use on supersonic aircraft wings and sounding rocket fins. For varying Mach numbers, these wings will lie outside and within the Mach cone.

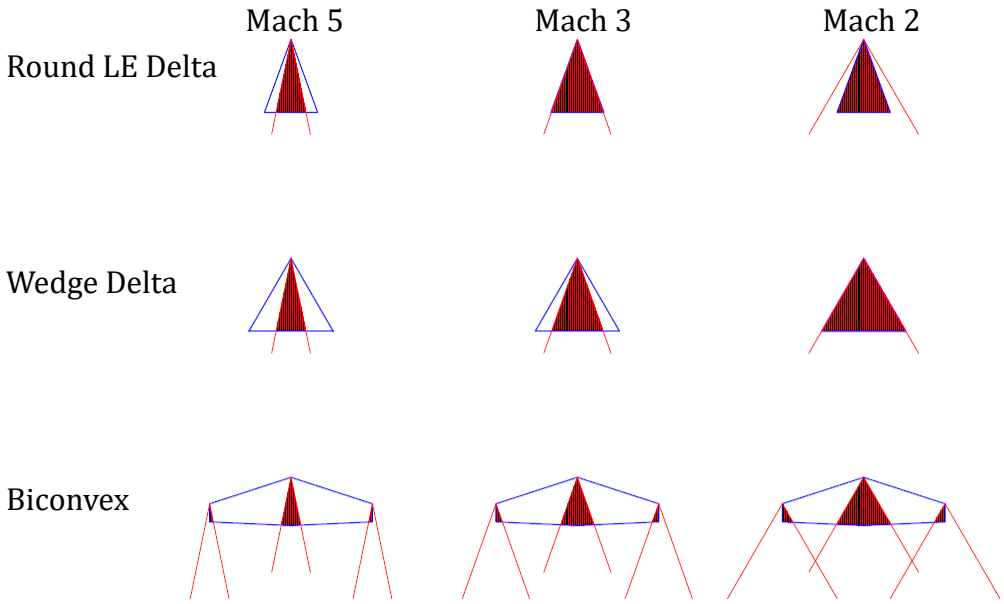

Figure 4-1 Mach cones on the chosen wing geometry.

4.1 Biconvex Wing

The first chosen wing geometry is a wing based upon the Lockheed F-104 Starfighter wing as described in (Friend and Safe 1972). The wing studied in this report has twice the span of that found in (Friend and Safe 1972) due to an error. Moderately swept with a sharp LE, this wing was used on the first operational Mach-2 aircraft. This wing is almost identical to those studied in (Ackeret 1925) with no compromises made to be more suitable for subsonic and transonic flight and falls mostly outside the Mach cone at all velocities. Therefore, it is expected that the analytical methods presented above will be in close agreement with the CFD results. It would also be expected that it will have its greatest performance at Mach 2. The geometry imported well and therefore no further refinement was needed ahead of running the simulations.

$\boldsymbol{\theta}$	6°
Reference Area(m^2)	18.21
∈	71.9
Max Thickness	0.03%
Thickness Position	50%
Chord (m)	3.96

4.2 Round LE Delta Wing

The second geometry chosen as part of this study is based upon the work in (Love 1949). This airfoil profile is of interest since the round LE defies one of the key assumptions of the theory above. It is worth simulating such a wing since it is much more representative if the types of wings found on operational aircraft which are designed to operate effectively below supersonic velocities. The high sweep of the planform is chosen in the hope such that at Mach 2 the entire wing will be within the Mach Cone. Although the sweep angle does not exactly match any wing found in (Love 1949), it is shown in the mesh independence study that the results are quite close to wing X in the NACA report which has a sweep angle of 17°. Due to the fineness of the wing tip and the curve of the leading edge, several surface mesh refinements were performed to gain an accurate representation of the geometry. These added a significant number of extra cells to the base mesh.

$\boldsymbol{\theta}$	N/A
Reference Area (m^2)	6.5514
∈	20°
Max Thickness	0.8% of chord
Thickness Position	18% of chord
Chord	6 metres

4.3 Wedge Delta Wing

The final geometry considered in this report is based on geometry found in (Ulmann and Bertram 1953). The wedge airfoil employed is one of the most common found in literature on supersonic aerodynamics. It is particularly well suited to analysis using shock-expansion but is equally suitable for linear analysis. One application of this type of airfoil is on sounding rocket fins. A sweep angle of 30° has been chosen such that the leading-edge parameter will be equal to 1 at Mach 3. As above, since there are wind tunnel test results available for this wing, correlations can be drawn between these results and the CFD results presented below. Similar to the Round LE wing the fineness aspects of the wing geometry were not represented accurately and several surface mesh refinements were performed to gain an accurate representation of the geometry.

θ	6°
Reference Area (m^2)	10.392
ϵ	30°
Max Thickness	0.5% of chord
Thickness Position	50% of chord
Chord	6 metres

5 Methodology

The simulations in this report were produced using Siemens StarCCM+ CFD software. SolidWorks CAD software was used to produce the fluid domains and wing geometries. Theoretical calculations were made using the MATLAB programming language.

5.1 Geometry Setup

Semi-Span models of the wing geometries were created in as a part in SolidWorks with their LE facing the opposite direction of the X-axis and their longitudinal axis aligned with the Z-axis. These were then opened in an assembly where a hemisphere of diameter 10x the chord of the delta wings region is created with the wing at the centre. The wing geometry is then extracted from the hemisphere using the cavity function. This hemisphere will form the basis of the freestream boundary. This hemisphere is then saved as a separate SolidWorks part and a in the Parasolid file format. At this stage a smaller hemisphere which served as a mesh refinement area was modelled also. No cavity function is used on this hemisphere.

The freestream geometry and the refinement geometry are then imported into StarCCM+ as a surface mesh.

5.2 Boundary Setup

Once imported the geometry is split into three surfaces, the hemisphere face, the wing and the curved surface of the hemisphere. These will form the basis of the regions and boundaries

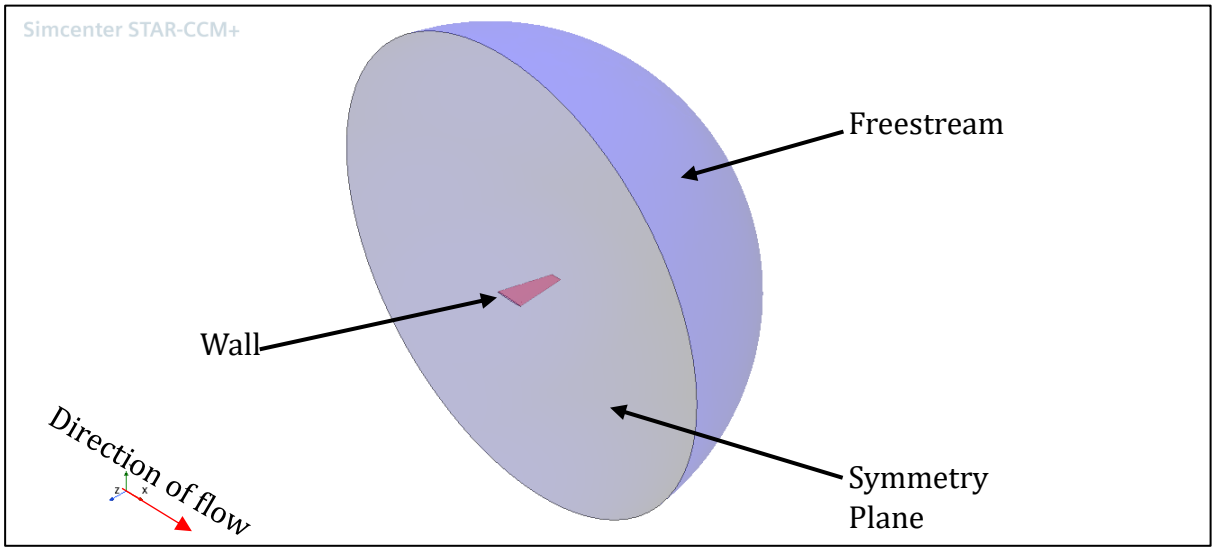

Figure 5-1 Boundaries defined in simulation.

used in the simulation. For the simulation of compressible flow a "Freestream" boundary condition is most suitable(Siemens 2022). This boundary emulates a large body of fluid surrounding an object. The diameter of this boundary must be defined such that there is no interference near the object of interest. To limit this, the freestream has been modelled as 10x the chord length of the wings. The flow conditions are set by specifying the Mach Number, Pressure and Temperature. The wing within this flow is set as a "wall" boundary and the hemisphere face as a symmetry plane. These boundary conditions were used on all static simulations in this report.

5.3 Physics and Initial Conditions

Due to the varying conditions of flow at Mach 2, 3 and 5 physics settings were adjusted for each velocity regime. Common across all simulations was the use of inviscid, compressible air as the working fluid. An inviscid model is used as the analytical theories used in the report all assume non-viscous flow. The fluid was simulated using International Standard Atmosphere values at 350000ft (Young 2018). The initial conditions can be seen in Table 5-1 below.

Although aerodynamic heating will not be analysed in this report, consideration has been given to the effect it may have on the physics of the working fluid. For simulations at Mach 2 the ideal gas model is used with a constant value of C_p. At velocities of Mach 3 and above, StarCCM+ suggests the use of a polynomial function of T to calculate the value of C_p (Siemens 2022). (Cross and West 2019) find that the default function supplied by StarCCM+ is accurate and does not require change. For simulations ran at Mach 5, the Equilibrium Air model is used which is a real gas model. When this model is selected the material properties are automatically calculated as functions of temperature and pressure(Cross and West 2019).

Table 5-1

Mach Number	Temperature(K)	Velocity(m/s)	Pressure(Pa)	Density(kg/m^3)
Mach 2	218.81	593	238042	0.376
Mach 3	218.81	889.5	238042	0.376
Mach 5	218.81	1482.5	238042	0.376

5.4 Solvers

The flow has been solved using the StarCCM+ Coupled Flow solver. This solver is better suited to compressible flow than the Segregated Flow Solver as it solves the mass, momentum and energy equations simultaneously(Cross and West 2019). The Coupled Flow Solver is particularly applicable to the cases in this report as it can use Inviscid Fluxes(Siemens 2022). For simulations ran at Mach 2 and 3, the ROE FDS scheme is used while at Mach 5 the AUSM+FVS scheme is employed. The AUSM+FVS scheme was specifically developed to handle the formation of shockwaves and prevent the "carbuncle" phenomena at high-

supersonic velocities (Liou 1996). All simulations are ran using a second order differencing scheme.

Working together with the flow solvers is the Adaptive Mesh Refinement model. This model allows for the gradual refinement of the mesh based on defined field function with StarCCM+(Siemens 2022). Shockwaves can be as little as 0.00000127 metres thin(Anderson 2003). Therefore, it can be difficult to mesh along a shockwave without creating an overly fine mesh, even if the position of the mesh is known. Capturing the form of the shockwave is very important as the sudden discontinuities have a major effect on the downstream flow.

The following definition has been utilised:

```
mag(grad($ {MachNumber}))*($ {AdaptionCellSize})
```

This function is given in the StarCCM+ tutorial "Adaptive Mesh Refinement: Hypersonic Flow" and refines the mesh at gradients of the Mach number(Siemens 2022). Utilising this method allows for a coarser base mesh which can then be refined exclusively where is necessary as the uniform and parallel flow between shock and expansion waves does not need a fine mesh to be resolved. The criterion inputs for the refinement were chosen through trial and error for each simulation as it was found that for certain combinations geometries and flow velocities, stronger gradients were produced which meant that smaller criterion were needed to refine the flow. The AMR solver was triggered every 100 iterations as it is necessary for the solver to act on a converged solution (Siemens 2022).

5.5 Overset Setup

An overset mesh with a defined motion was used to vary the angle of attack on the wing. Overset mesh motion sets a boundary between two overlapping regions, one being set a background region and a smaller overset mesh that encloses the body (Siemens 2022). In this simulation a small region containing the wing and the freestream region was set as the background. A rotation of 5 °/s was then set on the region enclosing the wing. An Implicit Unsteady simulation was defined with a 0.02 second timestep. Minimum and Maximum inner iterations were set to 20 and 50 respectively. All other continua settings were identical to the steady simulations.

5.6 Mesh Independence Study and Simulation Validation

Using the Round LE Delta wing, a mesh independence study was carried out to validate the legitimacy of the conducted simulations. As this wing is based on the work of (Love 1949) for which there is wind tunnel data, this will also serve as validation of the simulation.

The mesh independence study was undertaken following the guidelines specified on the "NPARC Alliance CFD Verification and Validation" website(NPARC 2021). Although this study hasn't been completed exactly as recommended, it has allowed for an informed decision to be made regarding mesh density.

It was found that the converged values of C_L and C_D did not vary much with increased mesh density. Therefore, the coarsest of the meshes will be used for all simulations at Mach 2 and 3.

The simulations were ran at a Mach number of 1.92 at a value of α of 4° and care was taken to match the Reynolds number given by (Love 1949). C_L is in excellent agreement with the windtunnel test data shown in Figure 10-4 for a wing with a value of ∈ of 17.91 °. C_D is less in line with the test data but still within a reasonable level of agreement.

6 Meshing

6.1 Part 1

An unstructured tetrahedral mesh was used as a base mesh on all simulations. Due to the inviscid nature of the flow, no prism layers have been employed. Two mesh refinements have been applied to the base mesh. On the surface of the wing a surface mesh refinement has been applied. In an area twice the chord length of the wing a volume mesh refinement has been applied. This volume refinement has been achieved using the refinement bubble defined in section X. The refinement near and on the wing is necessary both for the accurate calculation of aerodynamic forces and to allow the AMR solver to detect Mach gradient in the

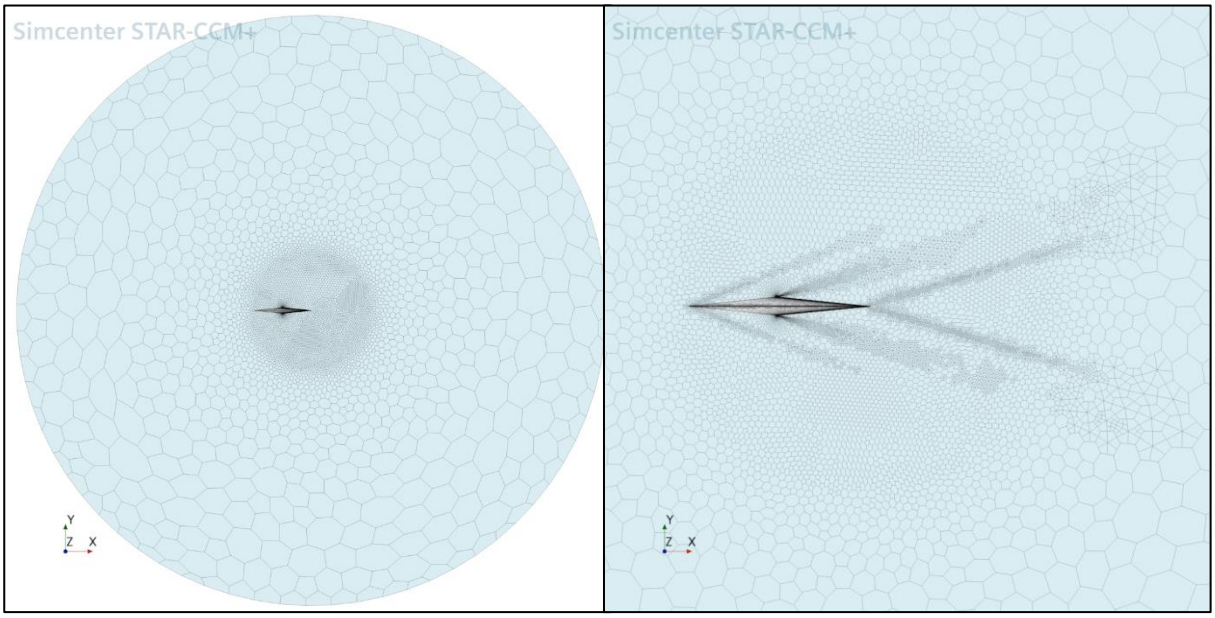

Figure 6-1 Mesh before and after AMR.

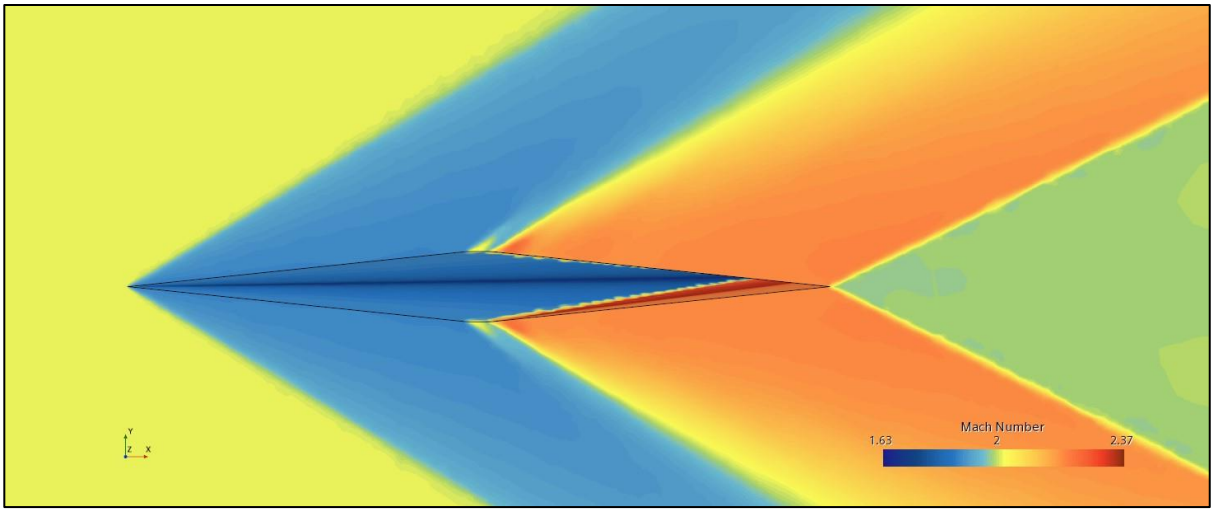

Figure 6-2 Result of a simulation without proper surface mesh, note the region of higher Mach number above the flat spot.

flow. A relatively course base Mesh can be used due to the utilisation of the AMR process. The mesh before and after the AMR process has run can be seen in Figure 6-1

The base mesh described above is similar to that used in the mesh independence study. Unfortunately, the surface meshing errors were not noticed at the time of the mesh independence study. Shown in Figure 6-2 is the result of meshing with an inadequate surface mesh. As specified above, it was necessary to manually refine certain features of the geometry on the delta wing configurations. This was done using a by defining a cylinder within StarCCM+. This part was then used as the input for a custom mesh control. The size of this part and the finesss of the mesh within it were refined until a suitable level of surface geometry was realised. The results of this can be seen in Figure 6-3.

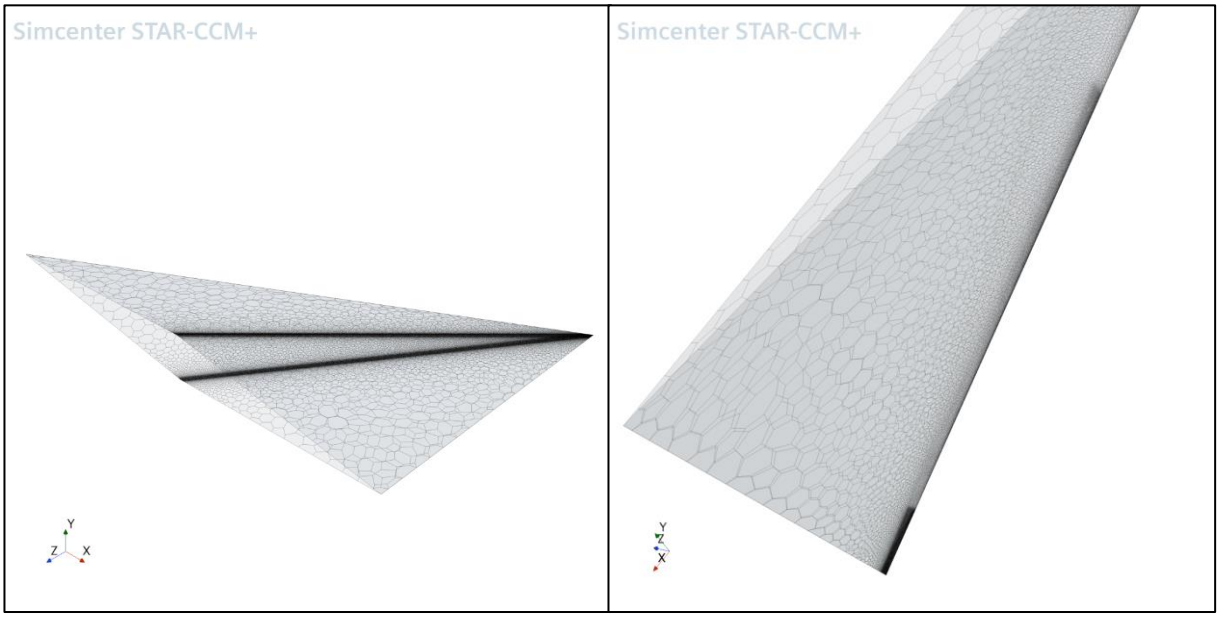

Figure 6-3 Surface Mesh Refinement on delta wings.

6.2 Part 2

The meshing parameters of this section are similar to that of Part 1, however some alterations have been made to facilitate the overset meshing. To facilitate adequate sharing of cells between the background and overset region a finer mesh was defined within the refinement hemisphere as seen in Figure 6-4.

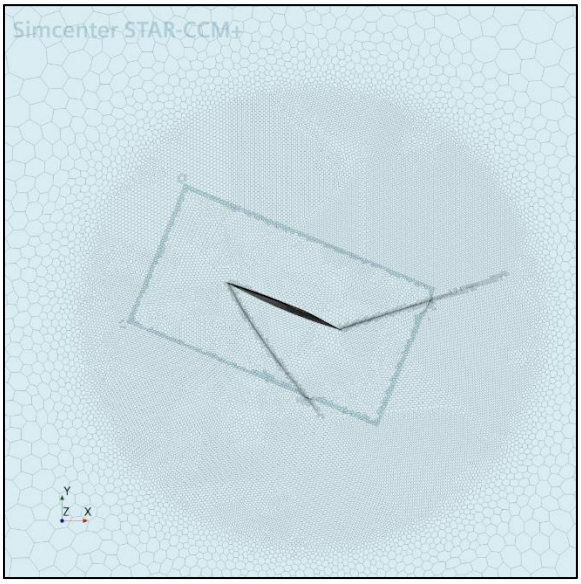

Figure 6-4 Overset Mesh

7 Zero-Lift Results

7.1 Shockwave Geometry

The ability for StarCCM+ to successfully detect and visualise shockwaves will be verified using the imagery produced by the simulation. The purpose of this section is to provide a summary of the shockwaves formed on the different geometry, full results can be found in the appendices.

Figure 7-1 shows the static pressure distribution at Mach 2 on the Biconvex Wing. Clearly visible are the Mach cones which closely resemble those sketched in Figure 4-1.

Figure 7-2 depicts the static pressure at a section at 1m of the span of the Round LE delta wing at Mach 2, 3 and 5. A detached shockwave can clearly be seen forming ahead of the leading edge with a high pressure build up ahead of the wing. Also visible is the shrinking angle of the shockwave angle with increasing Mach number.

Figure 7-3 depicts the Mach scalar on the upper surface of the Wedge Delta Wing. The shock cone forming coincident with the LE at Mach 2 can be seen. The very visible Mach number difference on the two surfaces of the wing can also be seen.

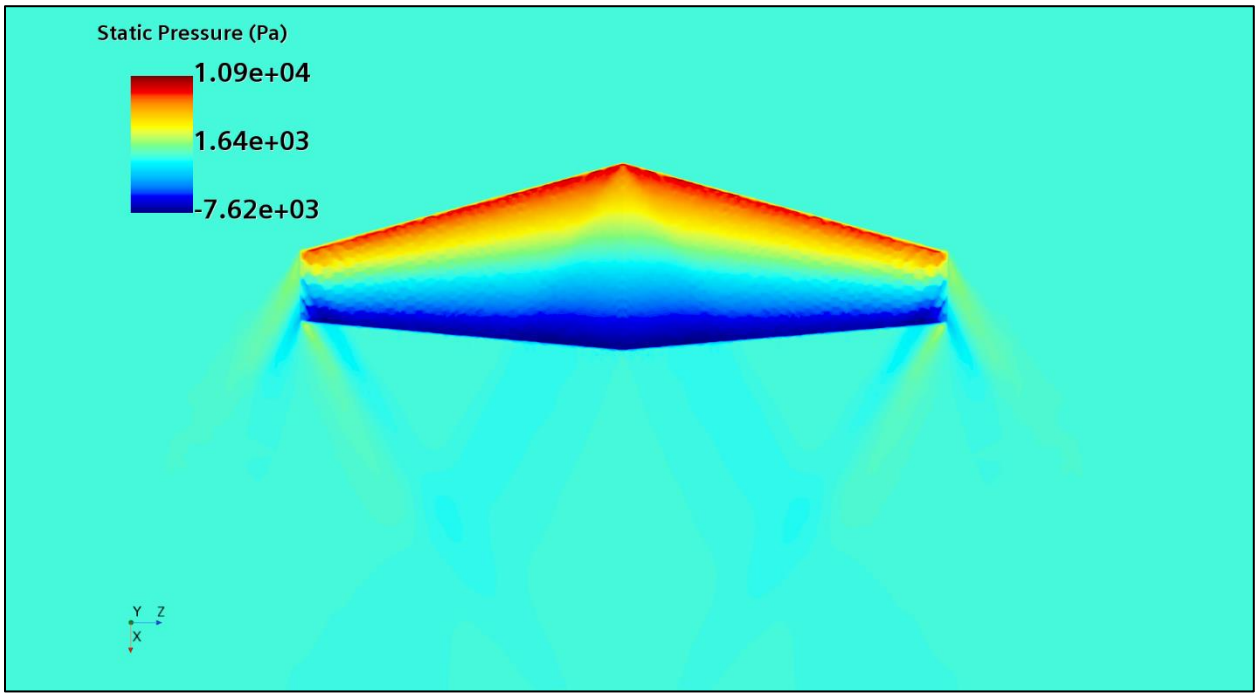

Figure 7-1 Static Pressure distribution on surface of Biconvex wing at Mach 2

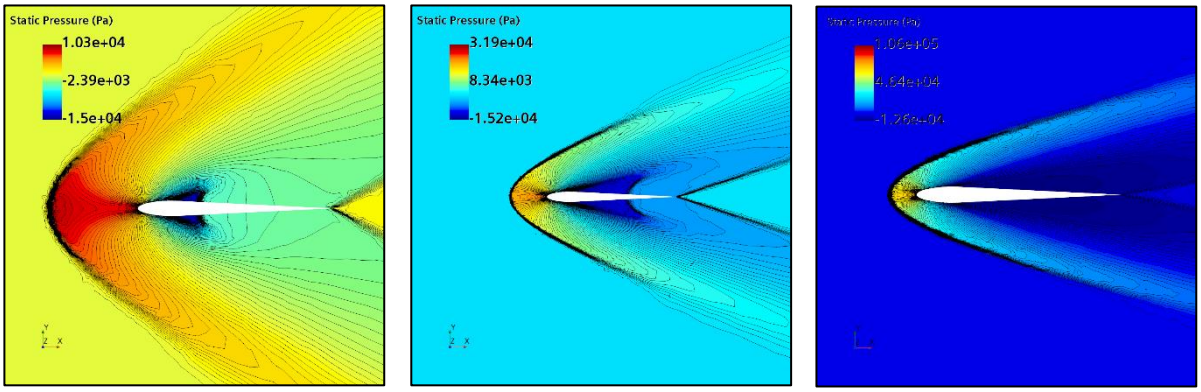

Figure 7-1 Pressure on Round LE Wing at a section taken at 1m of the span

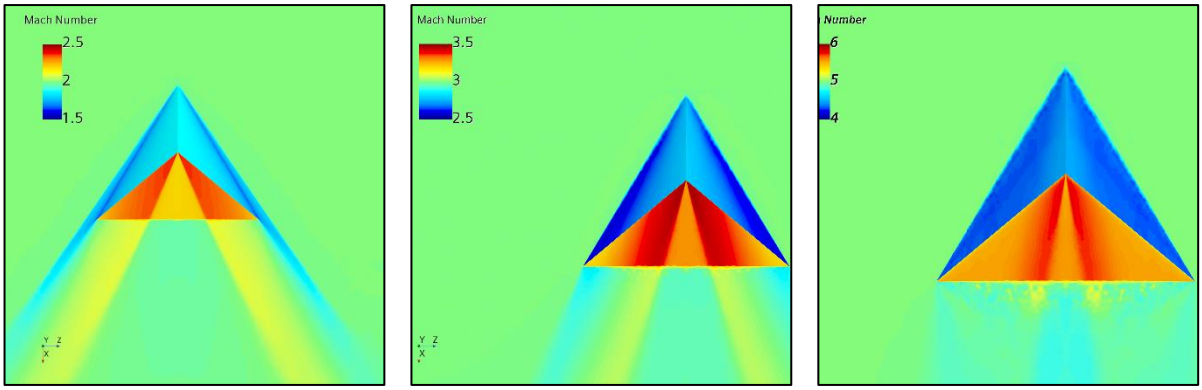

Figure 7-3 Mach Scalar on Wedge Delta Wing Upper Surface

7.2 Simulation and Theoretical Results

The following section will present some of the results of the data obtained from the simulation and the corresponding value calculated using Oblique Shock Theory.

The data was collected from the simulations using a line probe that was placed 0.05m above the wings for a distance of 10m. In this way the probe intersected the shock and expansion waves above the wing. Figures 7-2 and 7-3 show the variation of the shockwave angle with Mach number for both CFD and Oblique Shock Theory

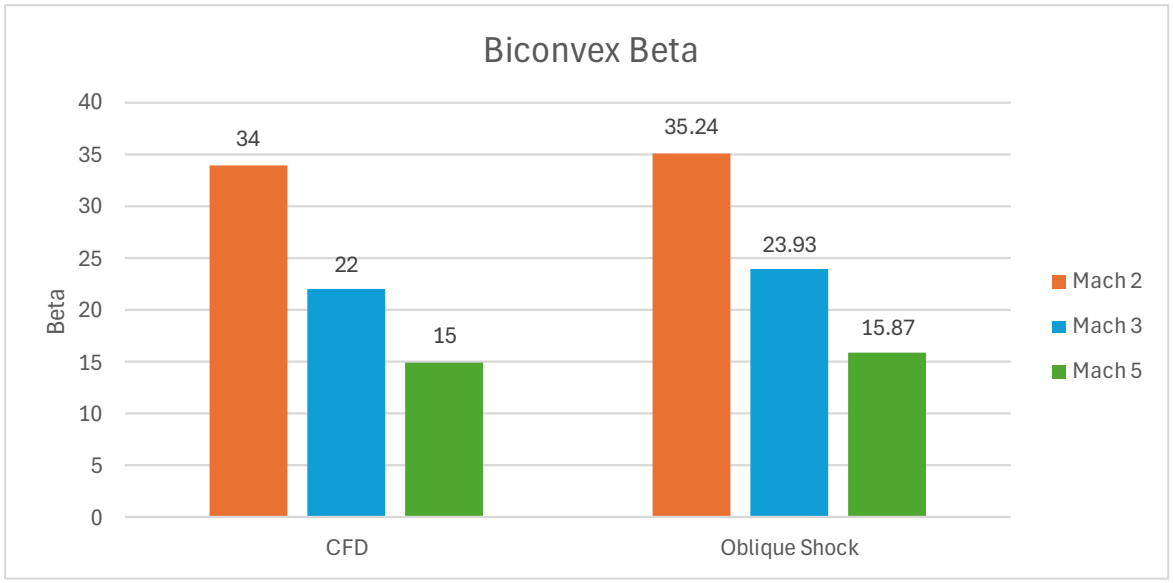

Figure 7-2 Angle of Shockwave on Biconvex Wing

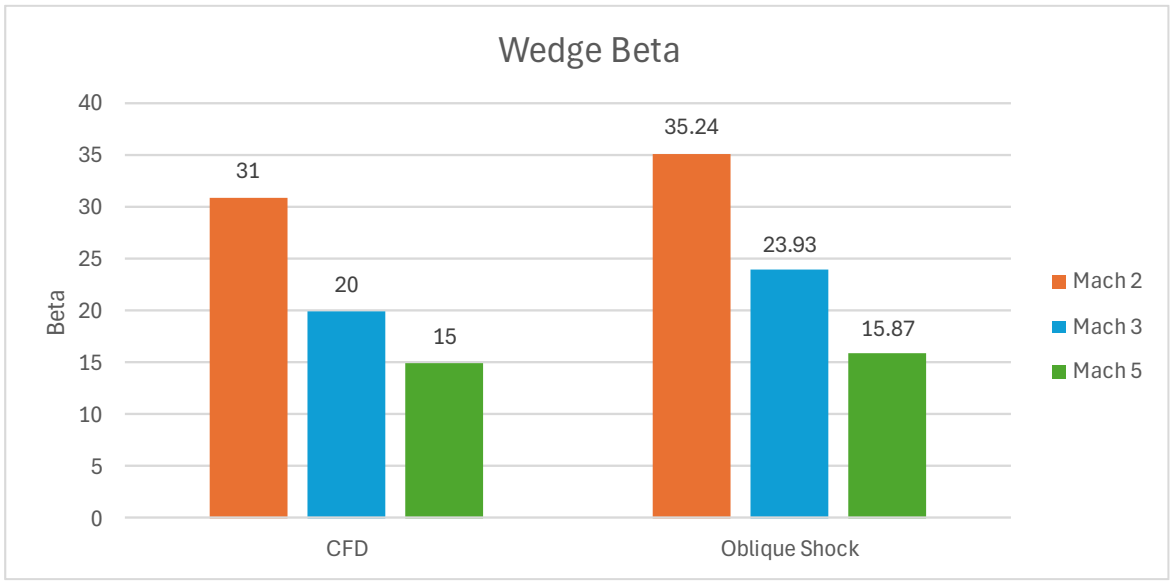

Figure 7-3 Angle of Shockwave on Wedge Delta Wing

Figure 7-4 shows the change of Mach number on the line probe as it passes through a shockwave above the Biconvex wing at Mach 3.

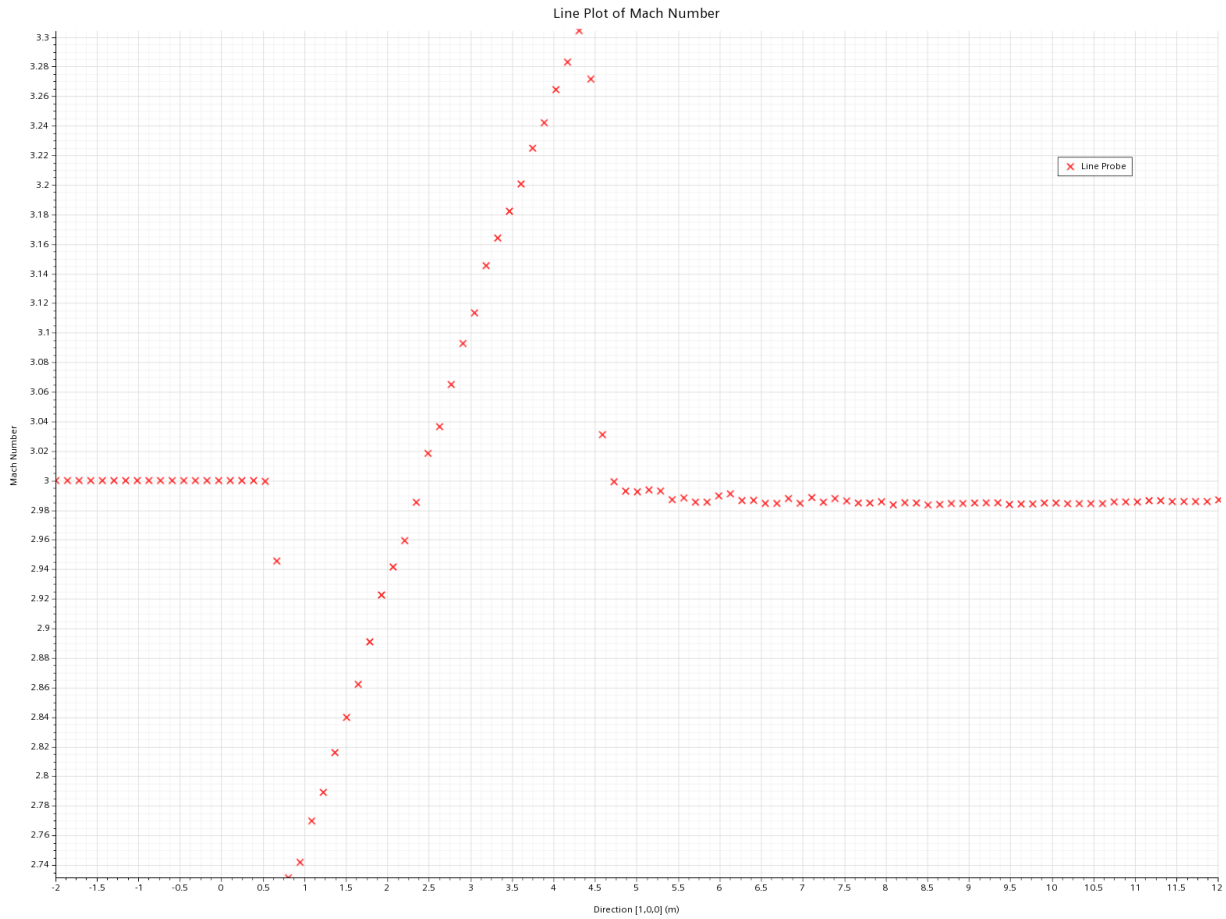

Figure 7-4 Mach number through shockwave.

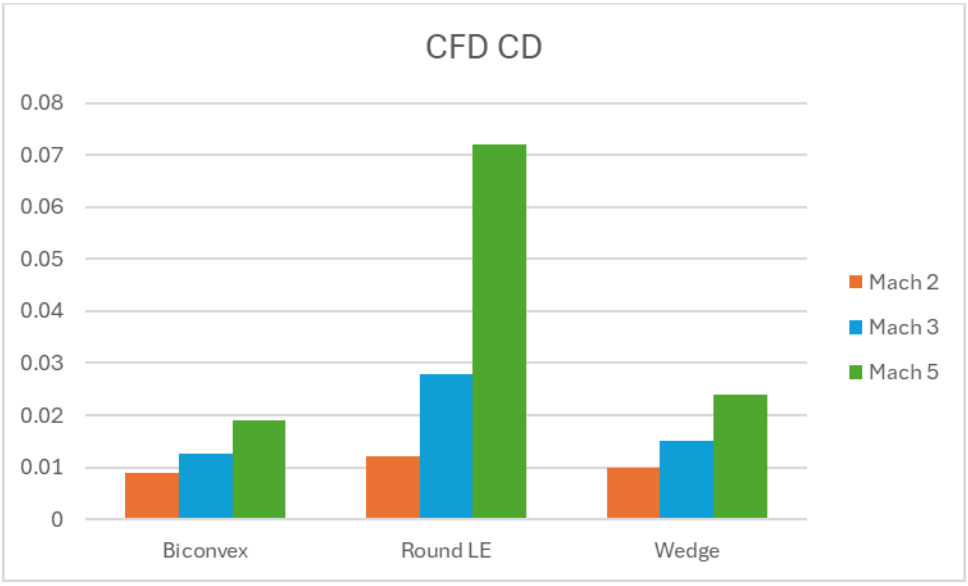

Figure 7-5 Coefficient of Drag on wings.

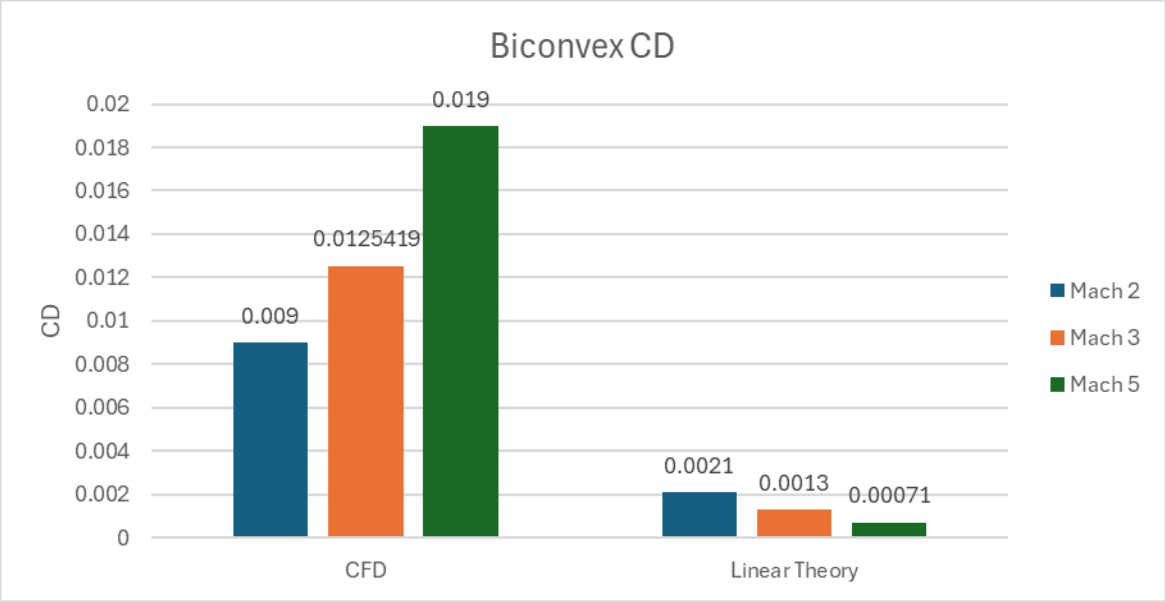

Figure 7-6 Linear vs CFD results on Biconvex wing.

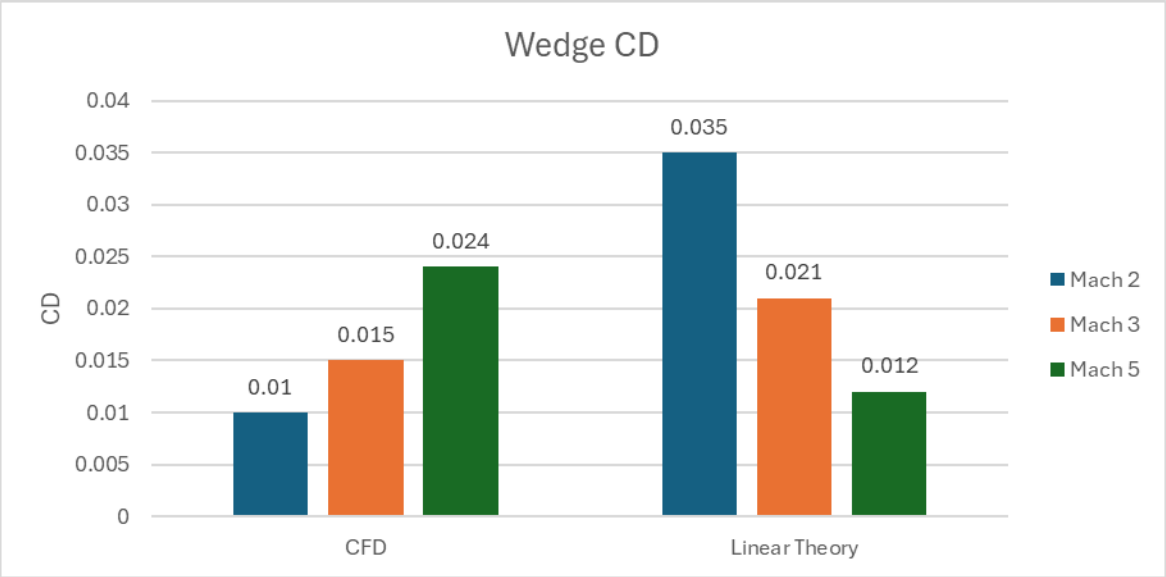

Figure 7-7 Linear vs CFD results on Wedge Delta wing.

Figure 7-5 shows the values of the coefficient of drag on the wings at zero lift for each of the three Mach numbers. The increasing wave drag with Mach number can be clearly seen.

Figure 7-6 shows the CFD results compared to the Linear theory for the Biconvex Wing. Clearly, they are not in agreement. Most likely there is an error in the Matlab code that has generated these values. This can be further proven by the reversed results shown for the Wedge Delta Wing in Figure 7-7.

8 Lifting Performance Results

Due to time constraints, the lifting performance simulations were only run at Mach 2. As the linear theory was in such poor agreement with the zero-lift values it was not considered for this section of the report.

Figure 8-1 shows the mesh and Mach scalar scenes after completing the simulation at an AOA and the resulting. The location of the shockwave and expansion waves can very clearly be seen in both.

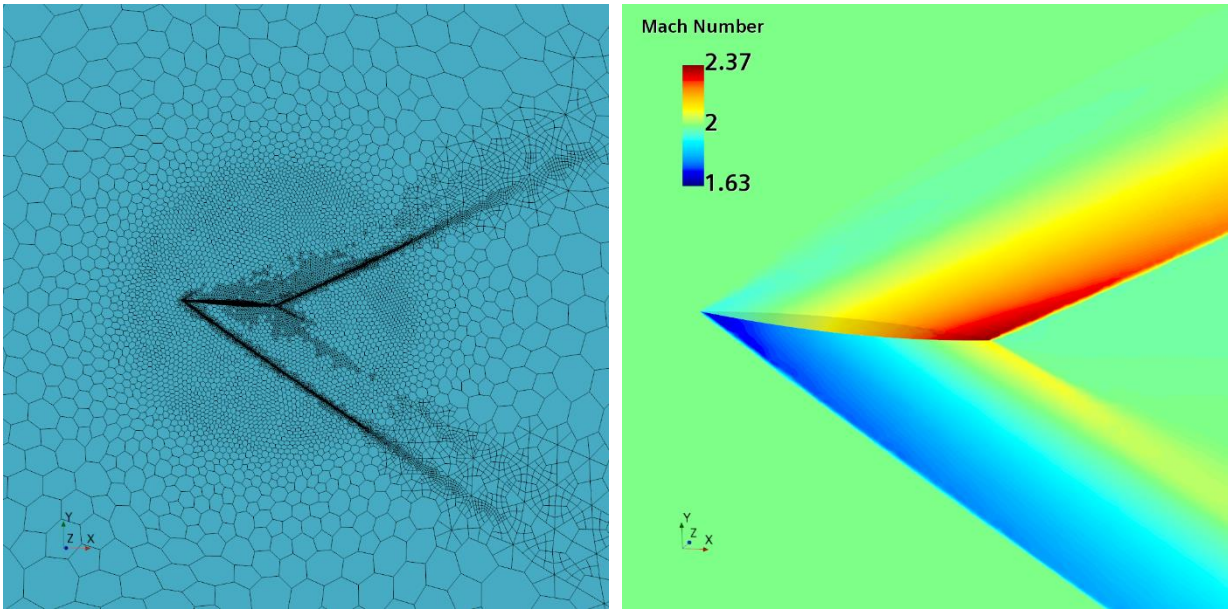

Figure 8-1 AMR mesh and Mach Scalar of steady simulation at an AOA.

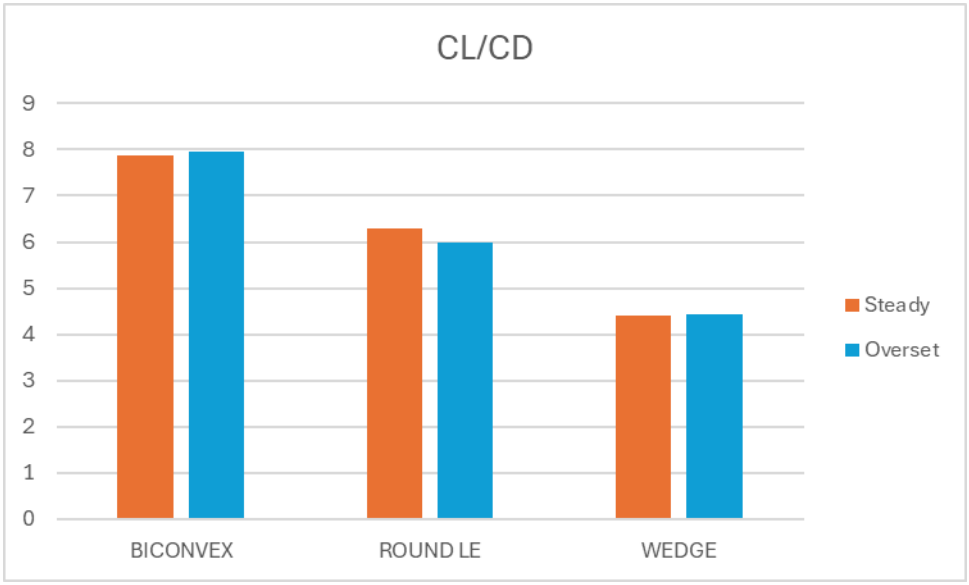

Figure 8-2 CL/CD Results for Overset and Steady AOA simulation

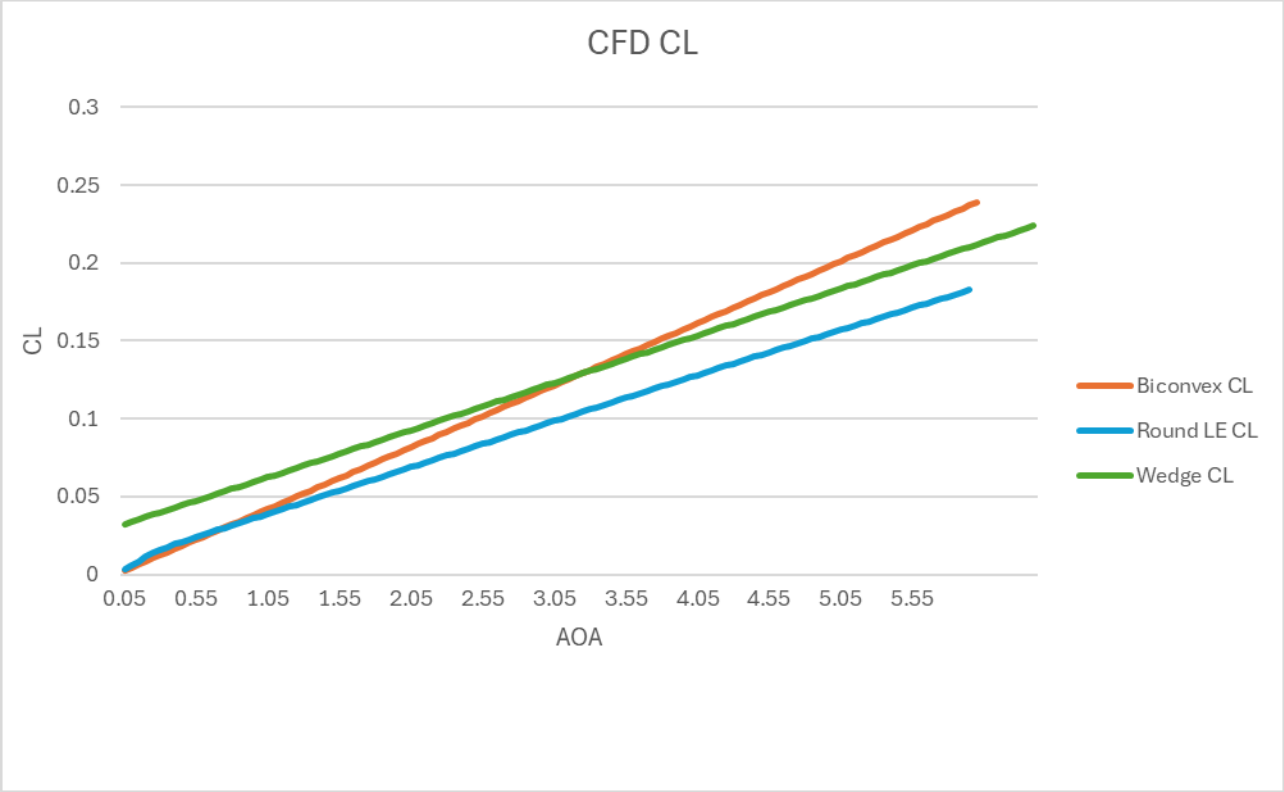

Figure 8-3 Overset Mesh Values for CL

Figure 8-2 shows the CL/CD values for the overset mesh and the steady simulation. They are in very close agreement with each other. It also not clear whether the steady or unsteady simulations are more accurate.

Figure 8-3 depicts the results of the overset mesh for CL. The Biconvex wing can be seen to generate the greatest C_L value.

9 Discussion

The main objectives of this project were to use the commercial CFD code, StarCCM+ to simulate the flow over supersonic wings and in doing so assess the accuracy and ease of using the tool for this purpose. Secondly the characteristics of different wings in supersonic flow would be examined.

It is clear from the snapshot of results that are presented above that the first task has been achieved. Shockwaves and expansion waves are clearly visible in the simulations and the software has successfully captured bow shock waves. The values produced by the simulations are in strong agreement with Oblique Shock Theory.

StarCCM+ has proven to be a versatile tool for the analysis of supersonic flow, the used of the Adaptive Mesh Refinement has allowed accurate supersonic simulations to be produced. Accessing aerodynamic force values and visualising the flow in an informative way was achieved with relative ease.

Although the linear theory could not be made to work, the oblique shock theory was used with high success and a deeper understanding of the governing aspects of supersonic flow has been achieved.

The wings used in this simulation have all provided interesting results. As expected, the Biconvex and Wedge Delta wings provided excellent shockwave and expansion waves for analysis. The most spectacular result was the detached shock that formed on the Round LE, Also, interesting was that the Wedge Delta wing had the lowest value for C_L/C_D. This may give credence to the leading suction that was explored in earlier papers in round leading edges.

An unexpected result is the lack of error between the CFD and the theory at Mach 3 and 5 as γ had been assumed to be 1.4 for all theoretical calculations while the CFD used models to predict this value at the higher Mach numbers. This suggests that for the conditions simulated, γ was equal to or close to 1.4 and the gas was close to ideal.

What was not expected was how closely the geometry formed by the shockwaves would resemble what was predicted in the theory.

10 Conclusion and Future work

In conclusion, a workflow for simulating supersonic flows using StarCCM+ has been developed. It has been shown that it is accurate when compared to the available theory.

The performance of the three wings was evaluated at Mach 2 and the Biconvex wing was seen to be the best performer.

Future work that could be undertaken should revolve around one aspect of this report and be given proper time to be fully explored this could include:

- Writing a working script for linear theory
- Exploring the performance of one of the wings at a range of AOA.
- Trying to recreate exactly previous windtunnel test results.

Future work could also expand to viscous simulations. Vortex shedding on a delta wing would be of particular interest. Flow separation at high angles of attack could be examined. Finally, a study which takes into account heating could be undertaken as supersonic aircraft will not crowd the skies unless suitable materials can be found to withstand such heat cycling.

Ackeret, J. (1925) *AIR FORCES ON AIRFOILS MOVING FASTER THAN SOUND*: NATIONAL ADVISORY COMMITTEE FOR AERONAUTICS.

Anderson, J.D. (1995) *Computational Fluid Dynamics: The Basics with Applications*, New York: McGraw-Hill, Inc.

Anderson, J.D. (2003) *Modern Compressible Flow With Historical Perspective*, 3rd ed., New York: McGraw-Hill.

Barrowman, J.S. (1966) *FIN - A computer program for calculating the aerodynamic characteristics of fins at supersonic speeds*, NASA Goddard Space Flight Center Greenbelt, MD, United States: NASA.

Bertin, J.J. and Cummings, R.M. (2014) *Aerodynamics for Engineers*, England: Pearson Education Limited.

Boom (2024) *XB-1 Takes Flight*, available: https://boomsupersonic.com/xb-1 [accessed 05/04/2024].

Cross, P.G. and West, M.R. (2019) *Simulation of Hypersonic Flowfields Using STAR-CCM+* China Lake, CA 93555-610: NAVAL AIR WARFARE CENTER WEAPONS DIVISION.

Drake, F. and Purvis, M. (2001) 'The Effect of Supersonic Transports on the

Global Environment: A Debate Revisited', *Science, Technology, & Human Values*, available: http://dx.doi.org/https://doi.org/10.1177/016224390102600406.

Friend, E.L. and Safe, W.J. (1972) *Flight Measurements of Buffet Characteristics of the F-104 Airplane for Selected Wing-Flap Deflections*, Flight Research Center, Edwards, Calif., 93523: NASA.

Hermeus (2024) *Halcyon*, available: https://www.hermeus.com/halcyon [accessed 05/04/2024].

Houghton, E.L., Carpenter, P.W., Collicott, S.H. and Valentine, D.T. (2013) *Aerodynamics for Engineering Students*, Sixth ed., Elsevier Ltd.

Jameson, A. (2012) 'Computational Fluid Dynamics: Past, Present and Future[SLIDESHARE]', in *Future Directions in CFD Research*, Hampton, VA.

Jones, R.T. (1945) *Wing Plan Forms for High Speed Flight*, Langley Memorial Aeronautical Laboratory, Va: National Advisory Commitee for Aeronautics.

Karman, T.v. (1947) 'Supersonic Aerodynamics-Principles and Applications', *Journal of the Aeronautical Sciences*, 14.

Liou, M.-S. (1996) 'A Sequel to AUSM: AUSM1', *JOURNAL OF COMPUTATIONAL PHYSICS*, 129.

Love, E.S. (1949) *Investigations At Supersonic Speeds of 22 Triangular Wings Representing Two Airfoil Sections for Each of 11 Apex Angles*, Langley Aeronautical Laboratory, Langley Air Force Base, Va.: NASA.

NASA (2024) *X-59 Debuts*, available: https://www.nasa.gov/feature/special-report-x-59-rollout/ [accessed 05/04/2024].

NPARC (2021) *Examining Spatial (Grid) Convergence*, available: https://www.grc.nasa.gov/www/wind/valid/tutorial/spatconv.html [accessed 28/02].

Schülein, E. and Guyot, D. (2006) 'Novel High-Performance Grid Fins for Missile Control at High Speeds: Preliminary Numerical and Experimental Investigations', in *RTO Applied Vehicle Technology Panel (AVT) Business Meeting Week*, Amsterdam, The Netherlands.

Siemens (2022) *Simcenter STAR-CCM+ Documentation*, 2022.1 ed., Siemens Digital Industries Software.

Tu, J., Yeoh, G.-H. and Liu, C. (2018) *Computational Fluid Dynamics: A Practical Approach*, Third ed., Elsevier Ltd.

Ulmann, E.F. and Bertram, M.H. (1953) *Aerodynamic Characteristics of Low-Aspect-Ratio-Wings at High Supersonic Mach Numbers*, Langley Aeronautical Laboratory, Langley Field, Va.: NASA.

Vincenti, W.G. (1951) *COMPARISON BETWEEN THEORY AND EXPERIMENT FOR WINGS AT SUPERSONIC SPEEDS* Ames Aeronautical Laboratory, Moffett Field, Calif.: NASA.

Wood, R.M. (1988) *Supersonic Aerodynamics of Delta Wings*, Langley Research Center, Hampton, Virginia: NASA.

Young, T.M. (2018) *Performance of the Jet Transport Airplane : Analysis Methods, Flight Operations and Regulations*, First ed., Hoboken, NJ, US: Wiley.

Zore, K., Ozcer, I., Munholand, L. and Stokes, J. (2020) 'ANSYS CFD Simulations of Supersonic and Hypersonic Flows', in *6th National Symposium on Shock Waves*, Chennai, India.

A. Biconvex Wing Section

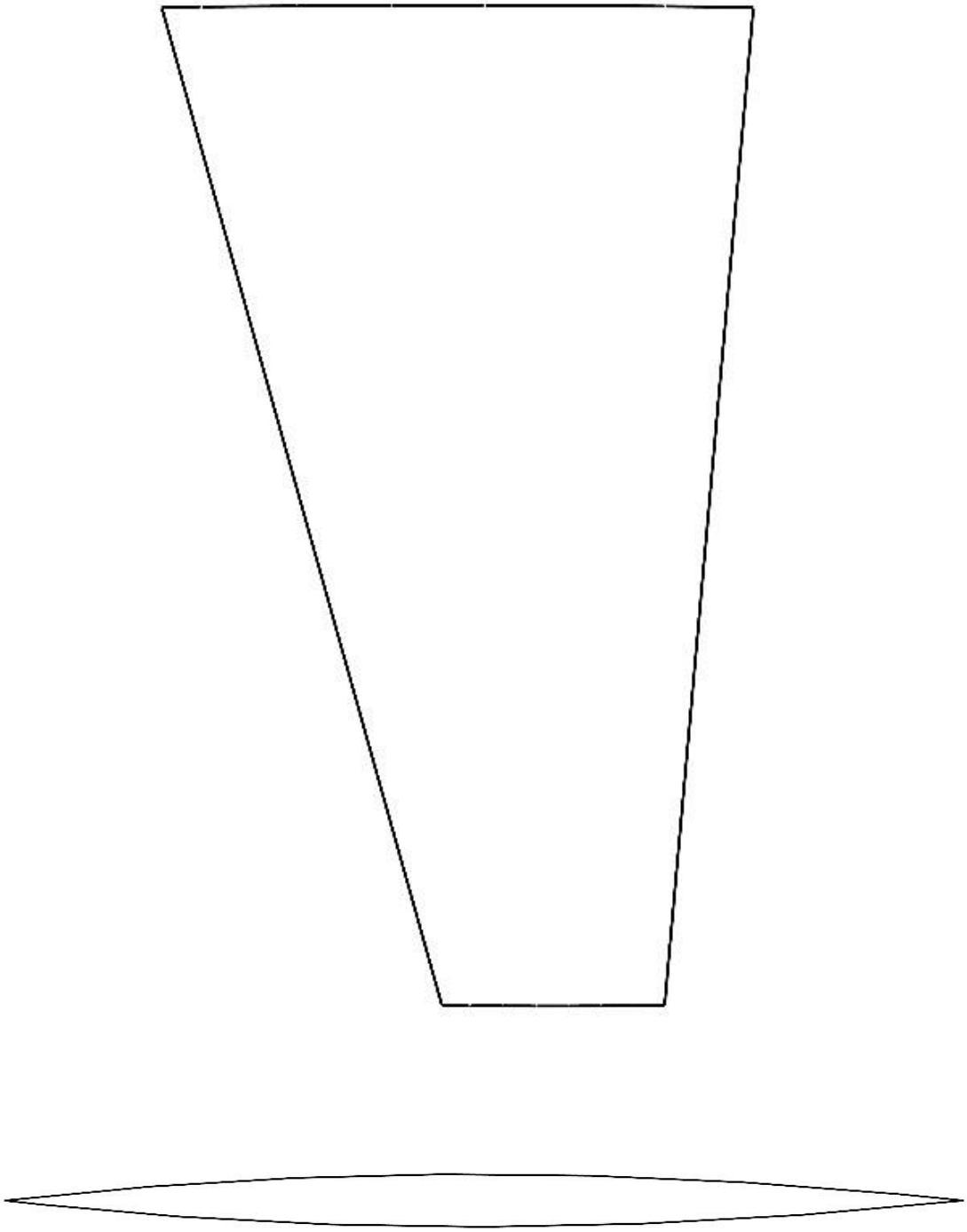

Figure A-1 Biconvex Wing Top and Side View

B. Wedge Delta Wing Section

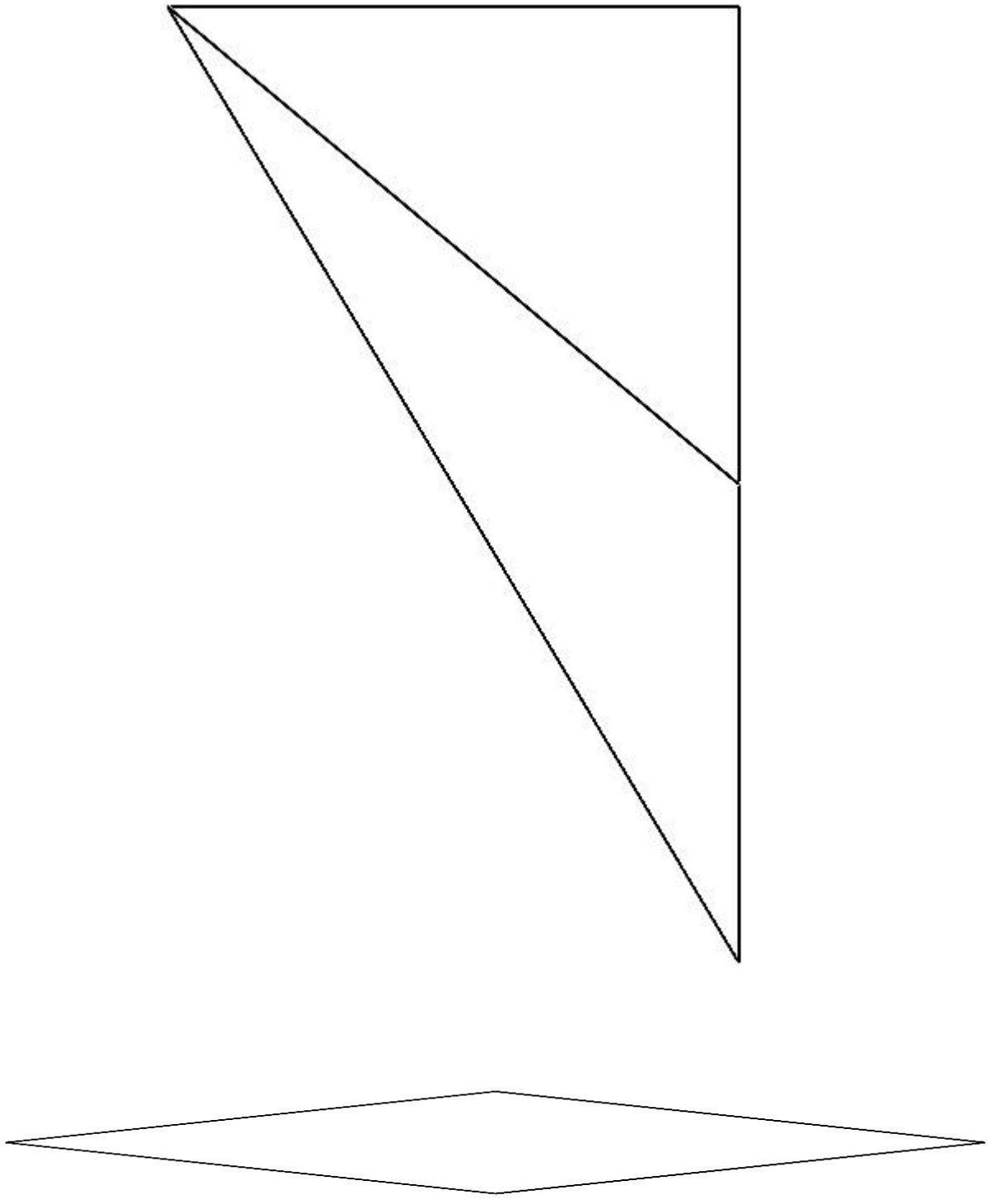

Figure B -1 Wedge Delta Wing Top and Side View

C. Round LE Delta Wing Section

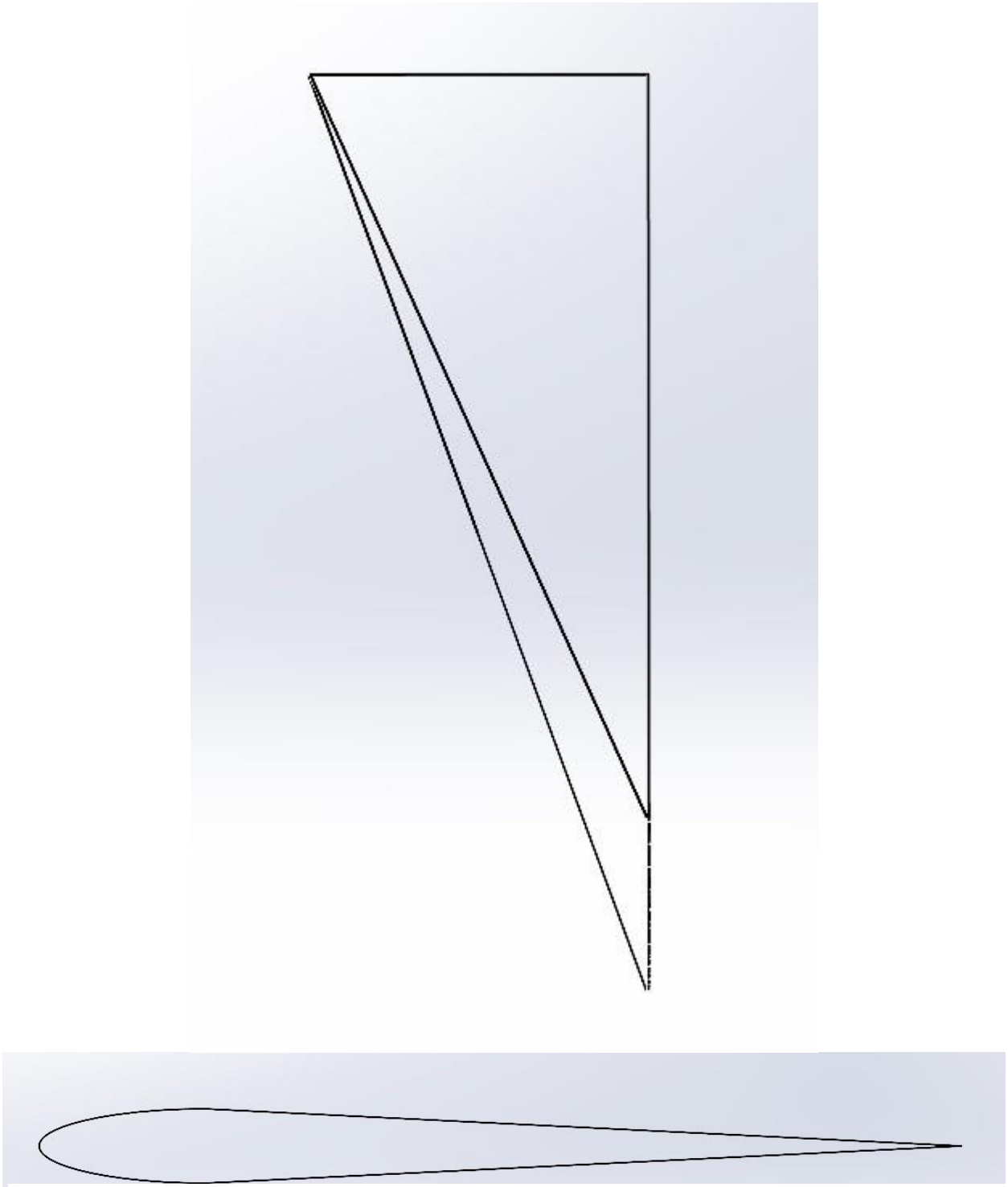

Figure C -1 Round LE Wing Top and Side View

D. Wing Renders

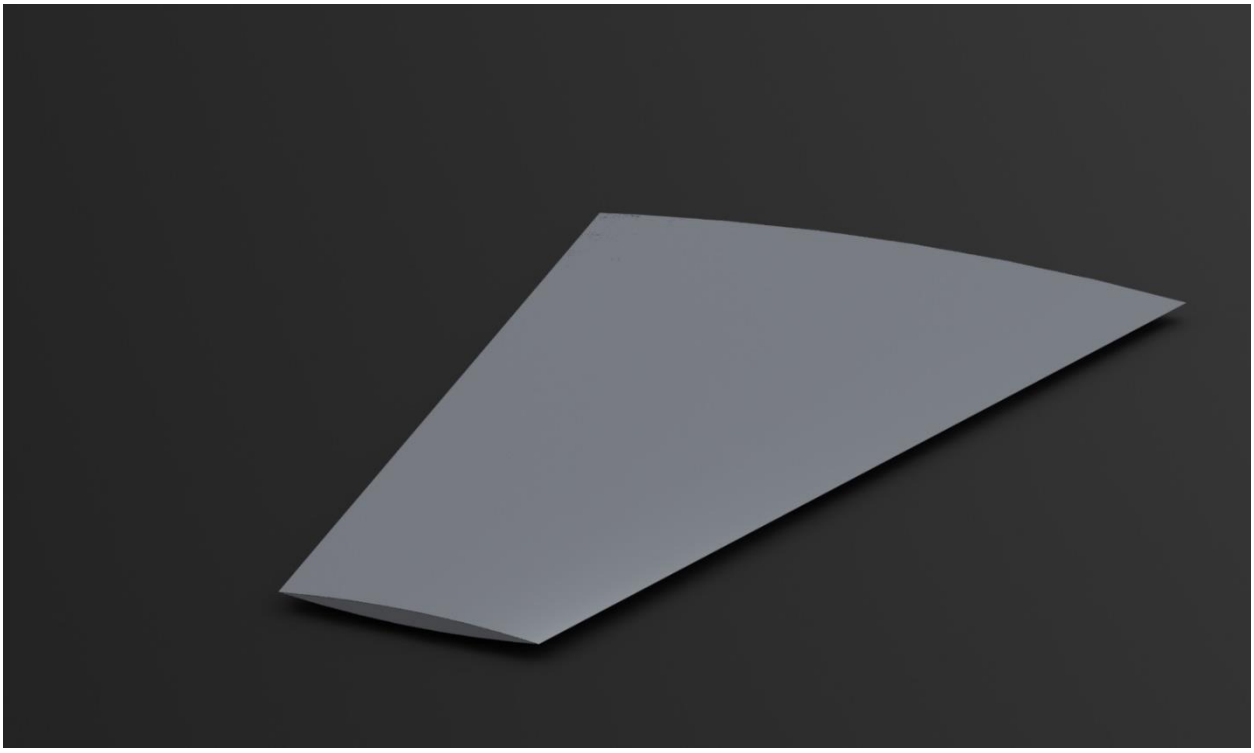

Figure D-1 Biconvex Wing Render

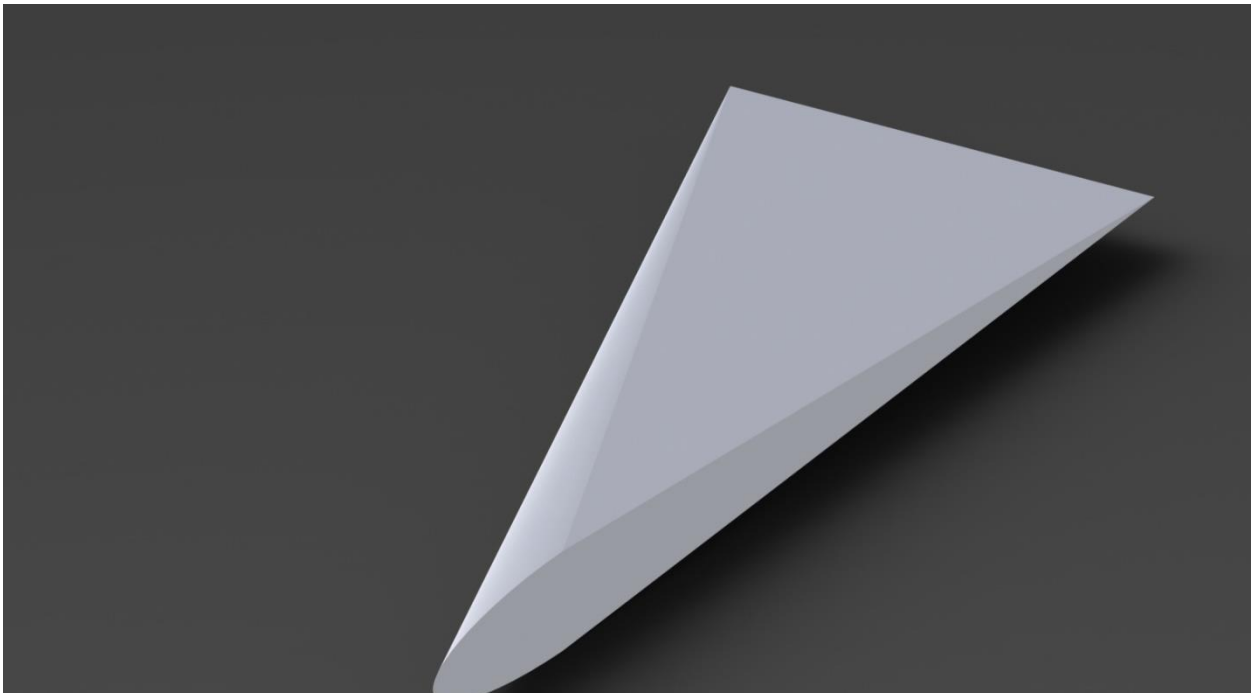

Figure D-2 Round LE Wing Render

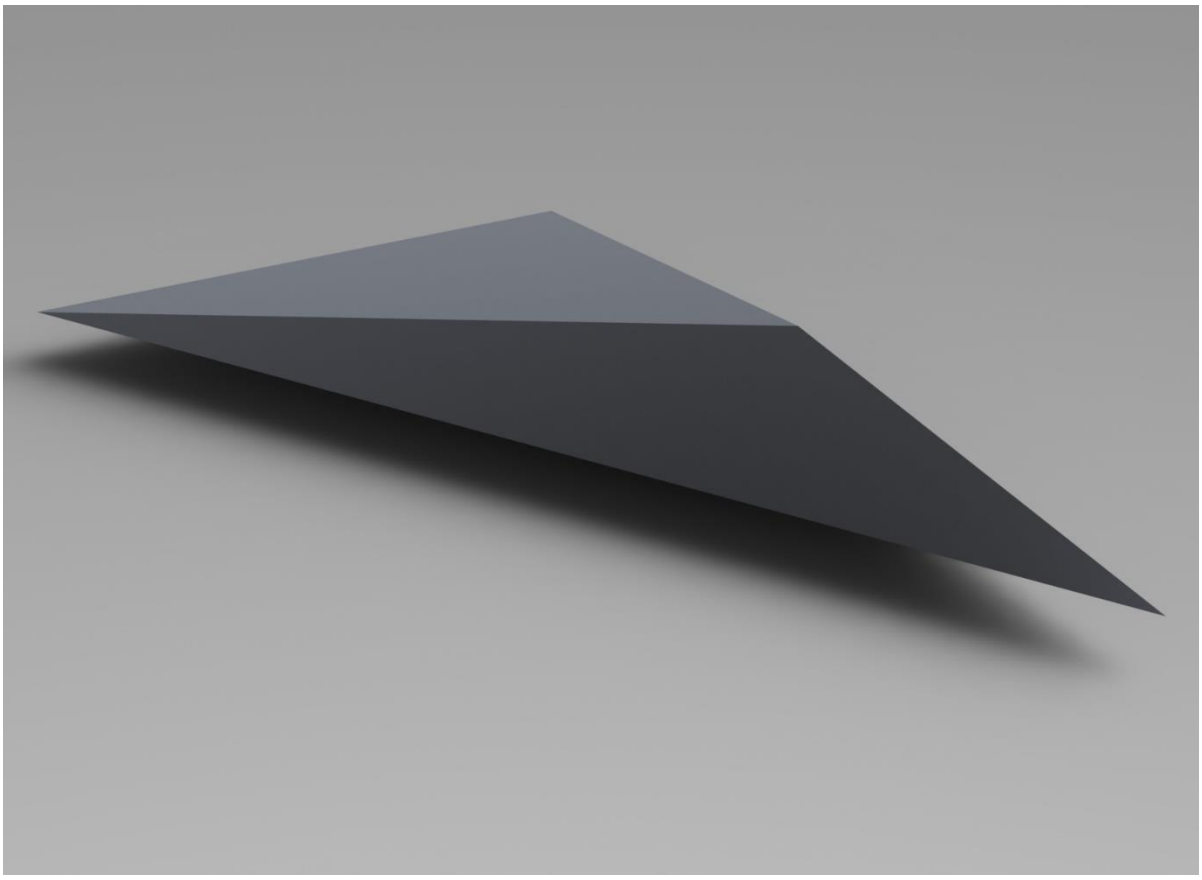

Figure D-3 Wedge Delta Wing Render

E. Volume Rendering on Round LE Delta Wing at Mach 2

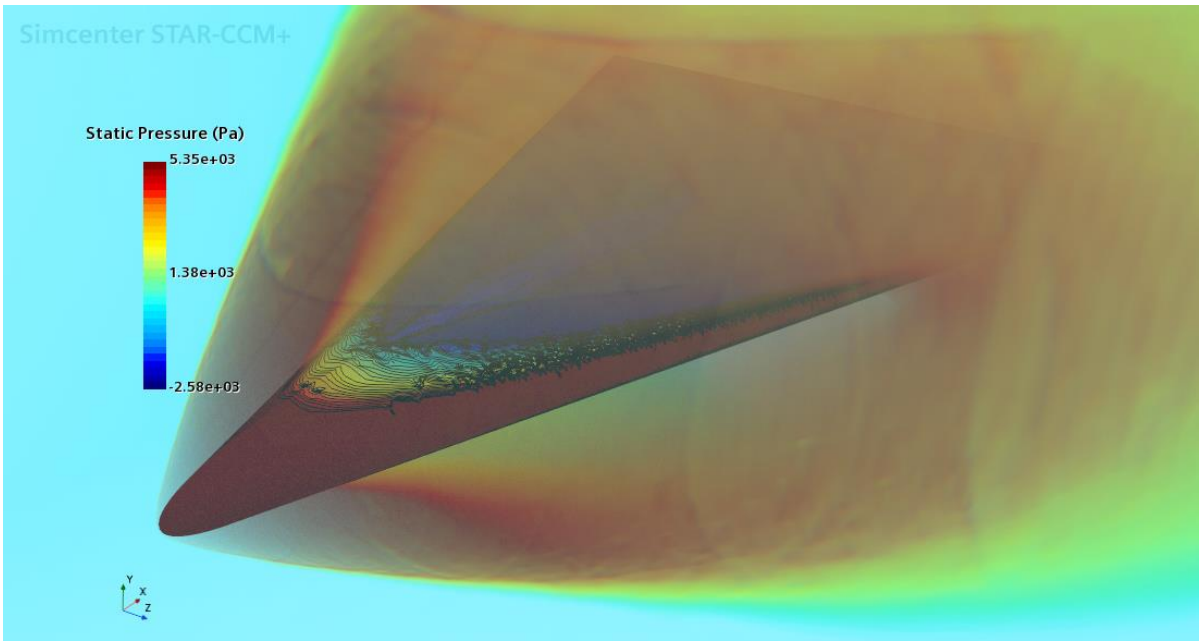

Figure E-1 Volume Rendering of Shockwave

F. Section Showing Conical Flow on Wedge Delta Wing at Mach2

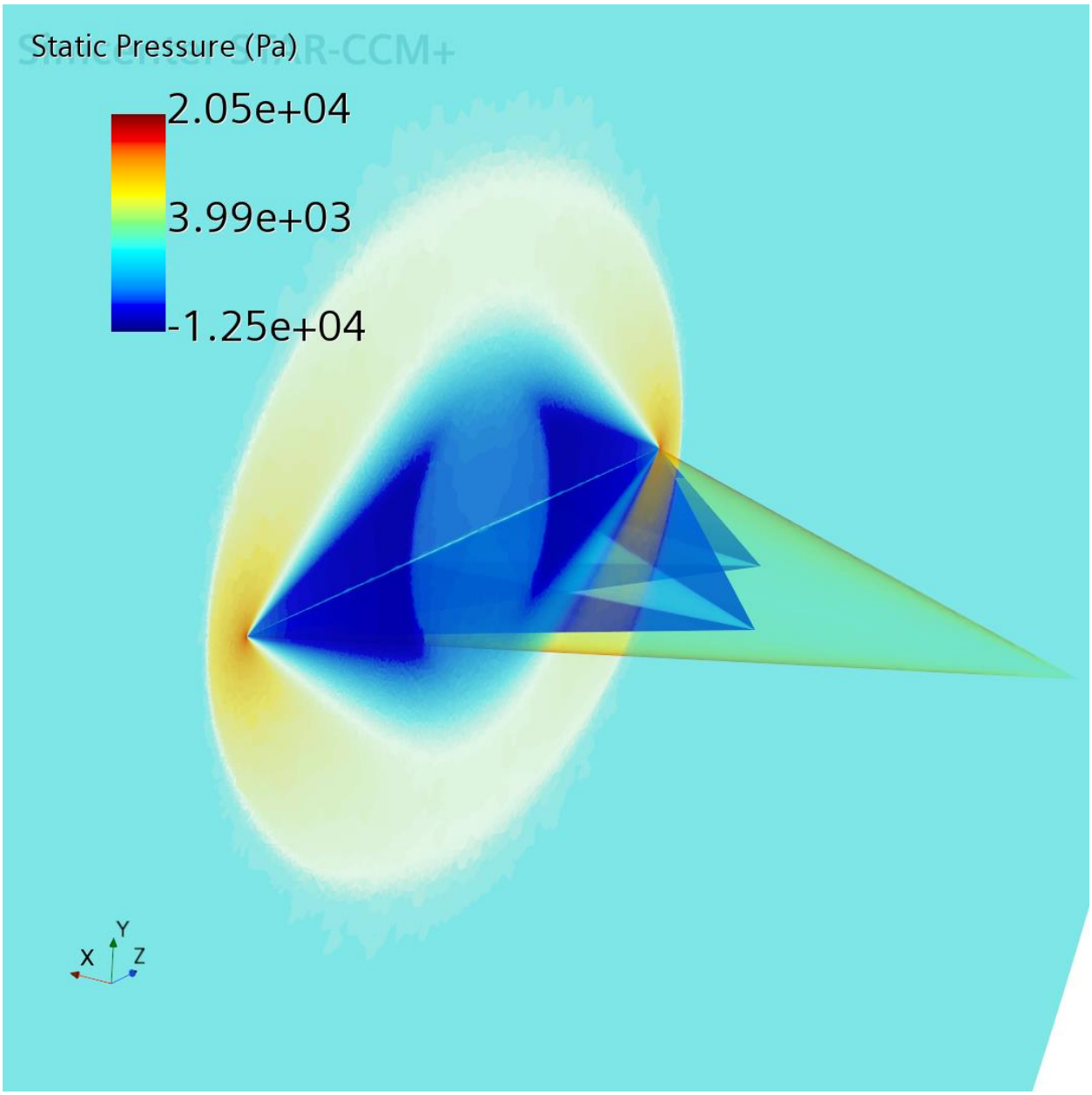

Figure F-1 Section view showing Mach cone downstream of wing

G Pressure and Mach Distribution on Wing Surface

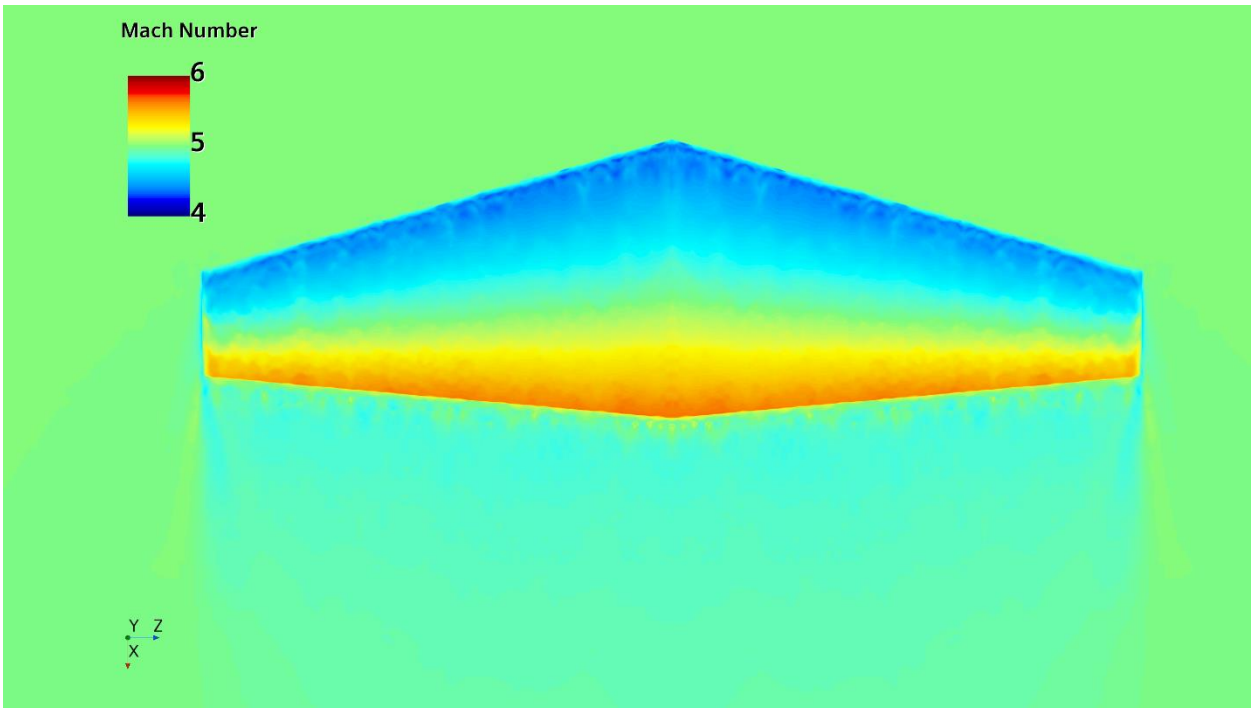

Figure G-1 Mach Scalar on Biconvex Wing at Mach 3

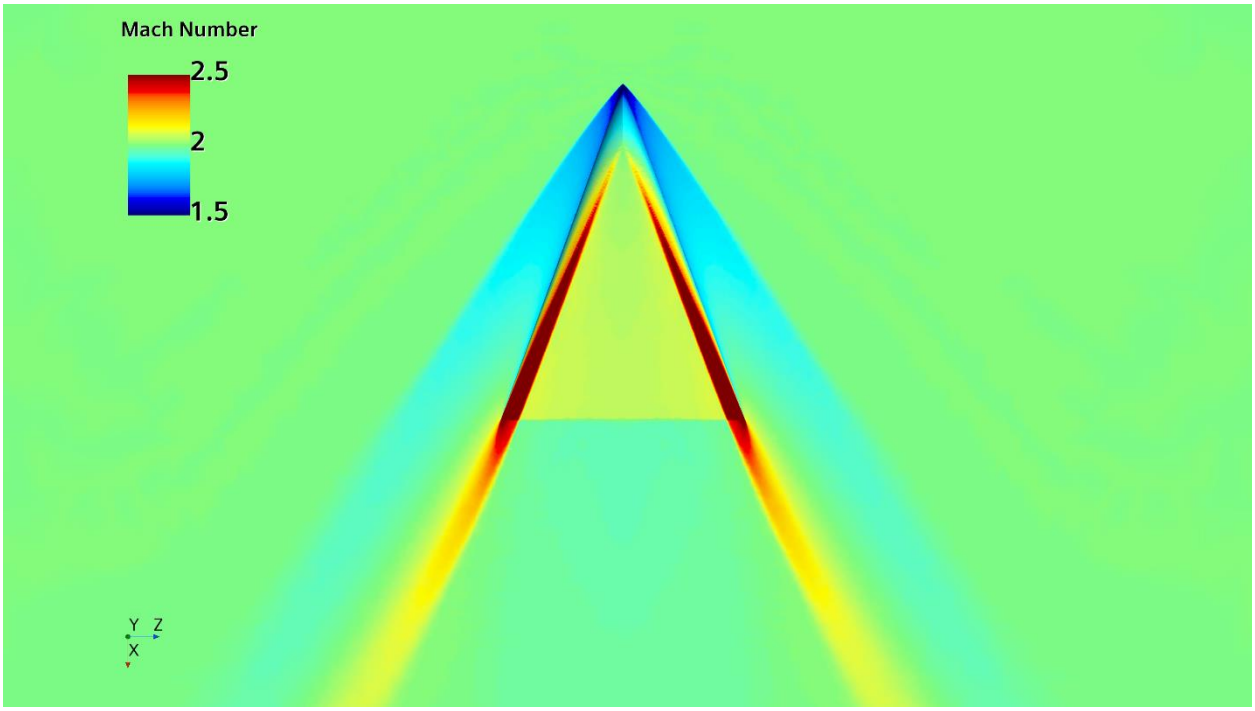

Figure G-2 Mach Scalar on Round LE at Mach 2

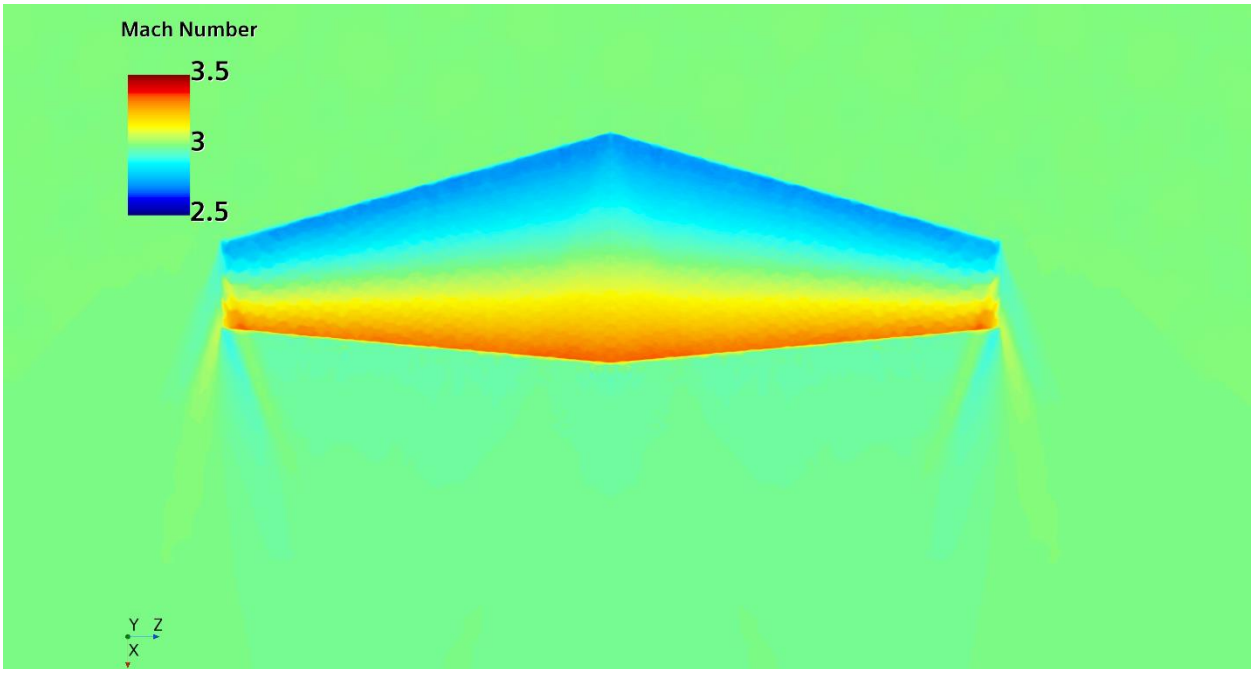

Figure G-3 Mach Scalar on Biconvex Wing at Mach 3

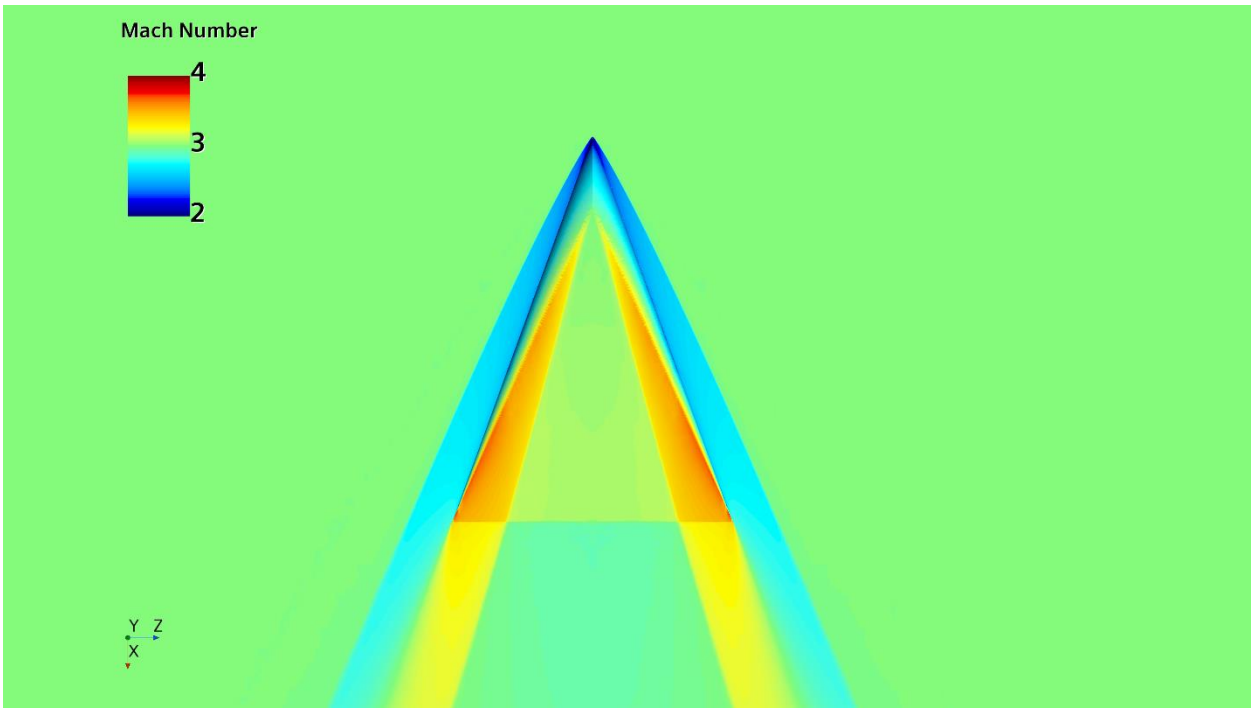

Figure G-4 Mach Scalar on Round LE Wing at Mach 3

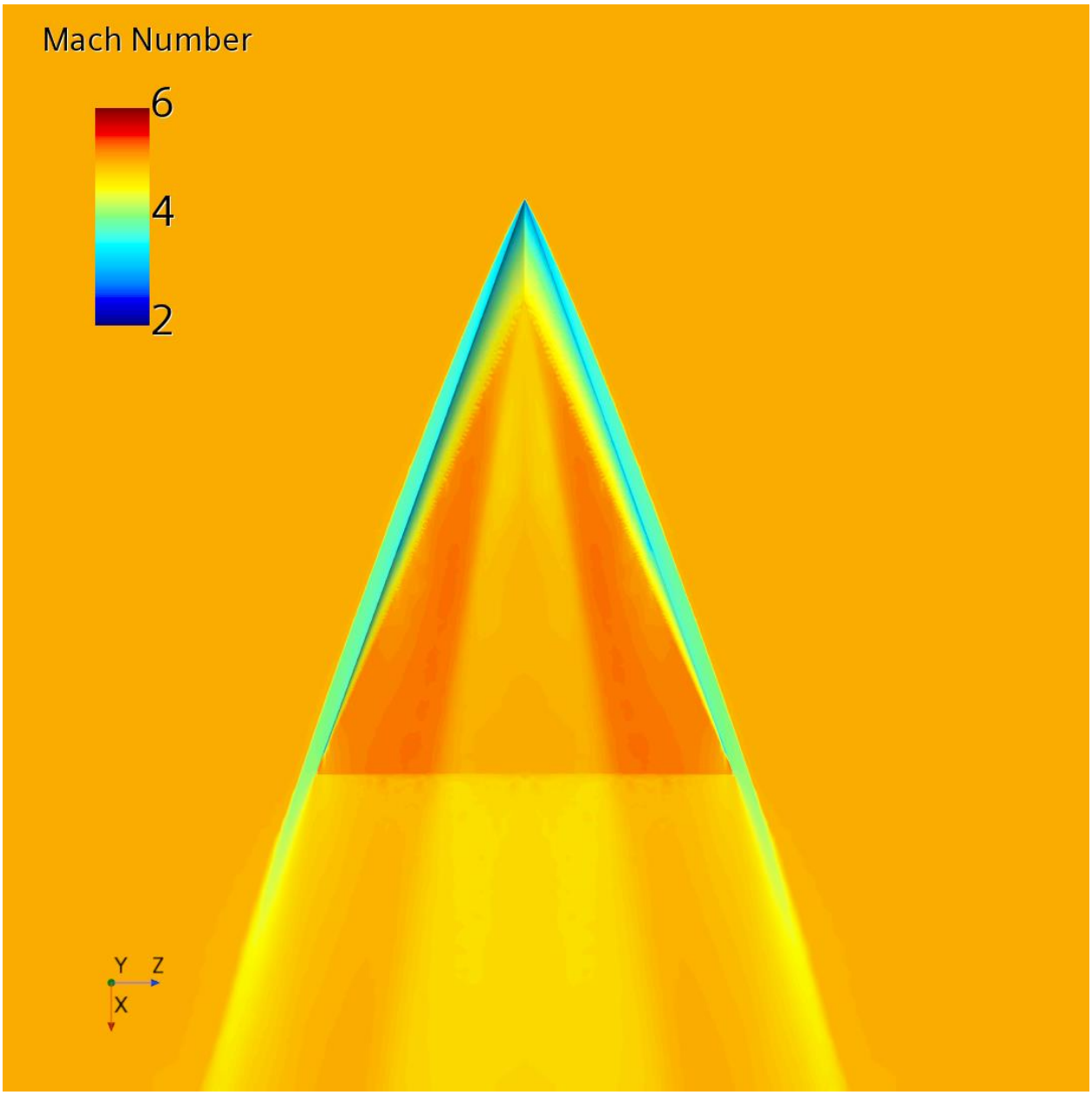

Figure G-5 Mach Scalar on Round LE Wing at Mach 5

H Root Section of Wings

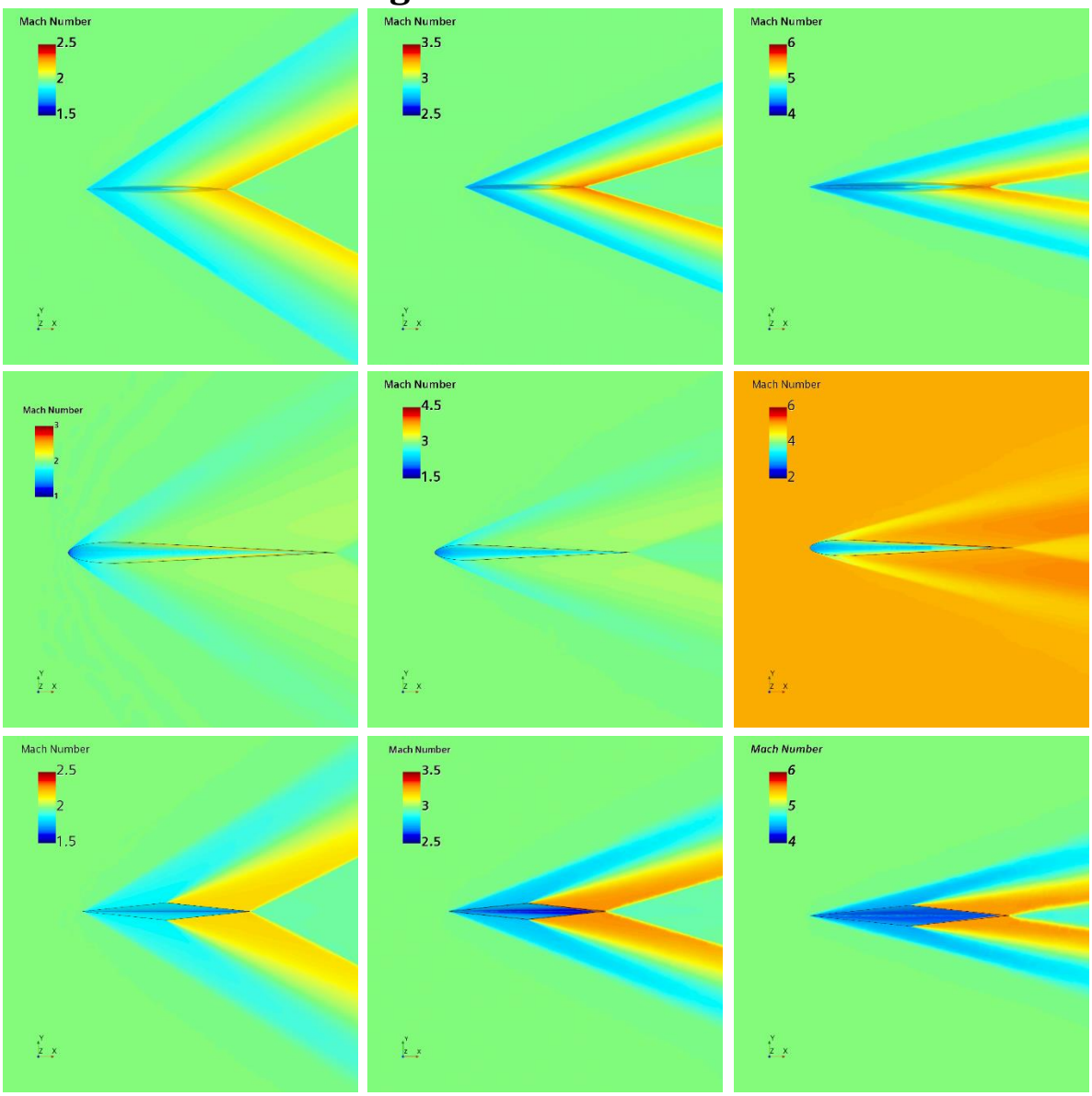

Figure H-1Mach Scalar at root section of Wings

I Section at 1m of Span of Wings

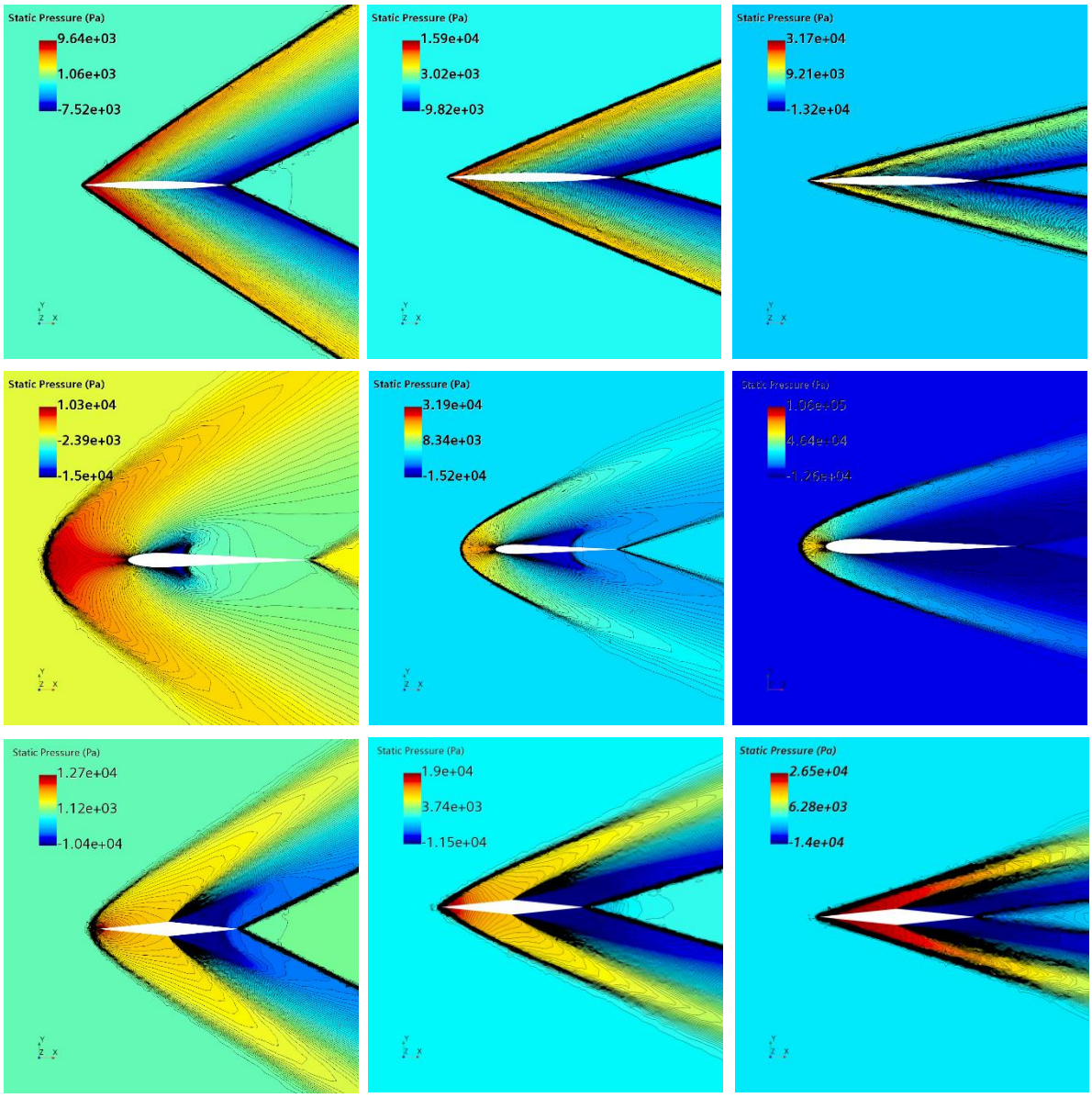

Figure I-1 Static Pressure Scalar at 1m of wing span

J Results of CFD and Oblique Shock Theory

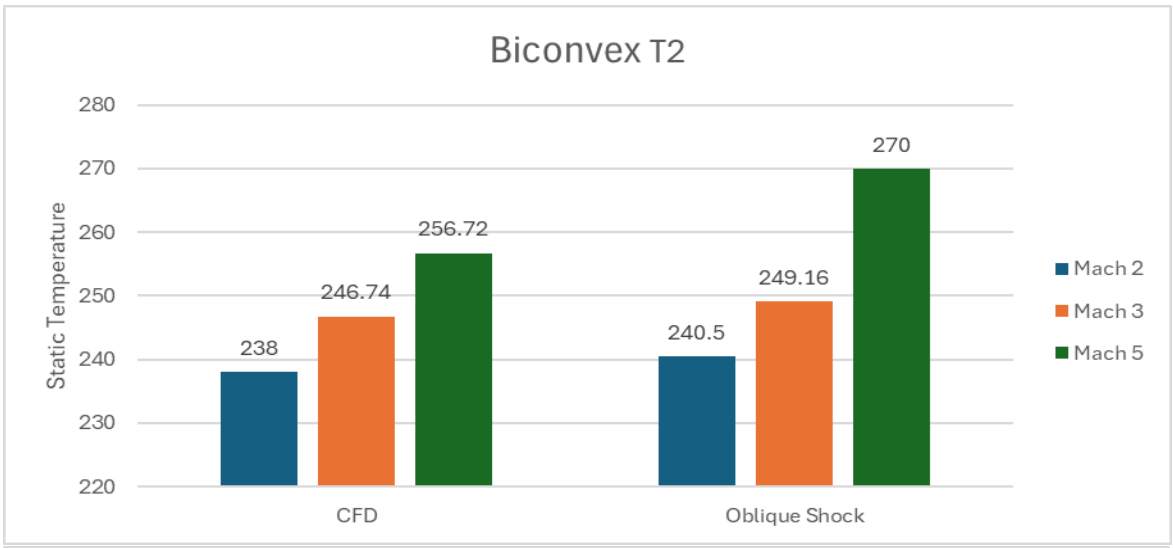

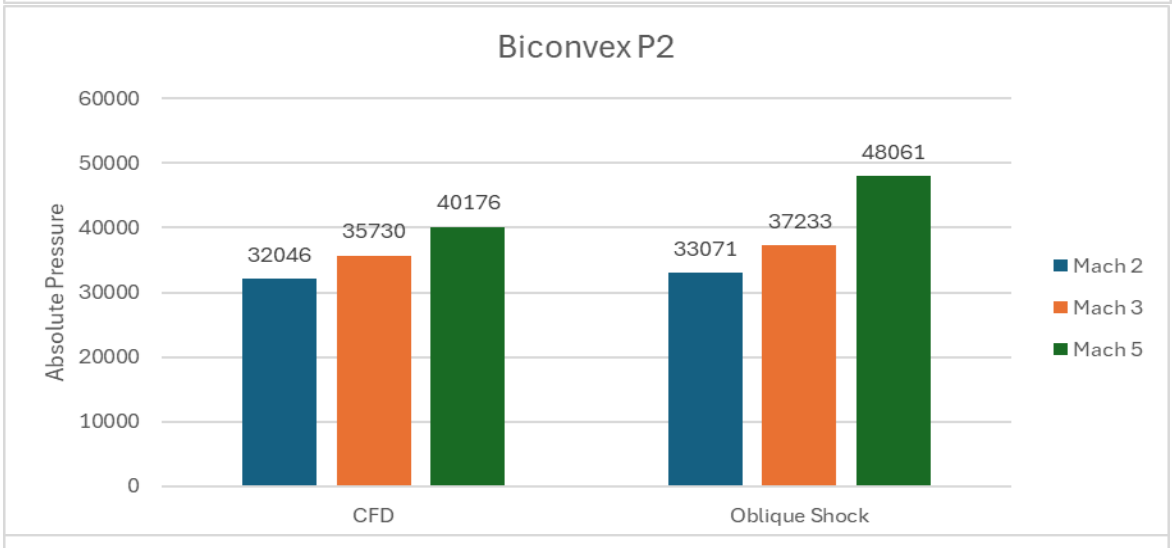

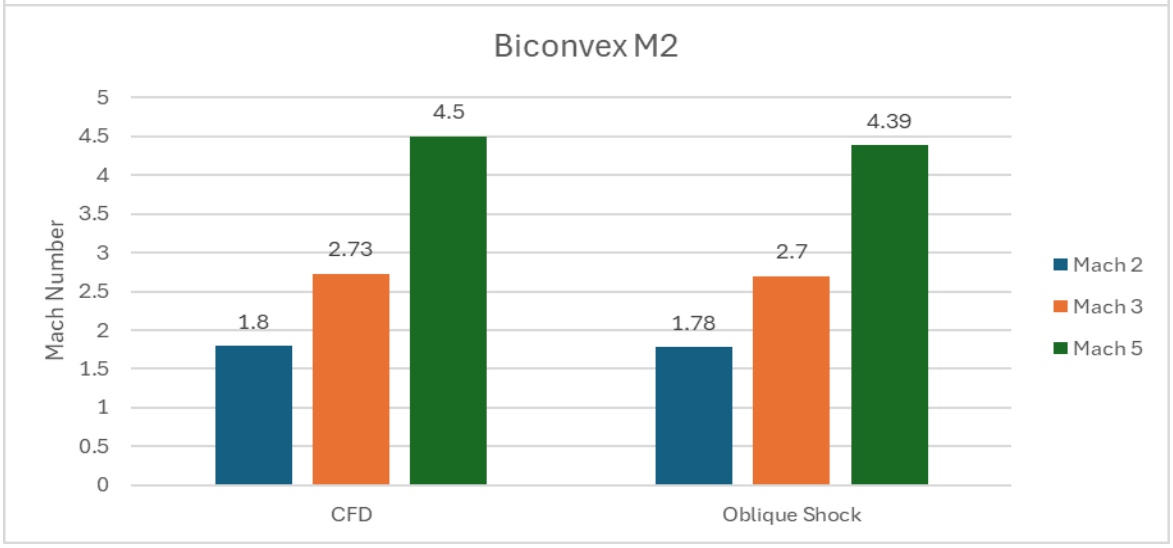

Figure J-1 Biconvex Results

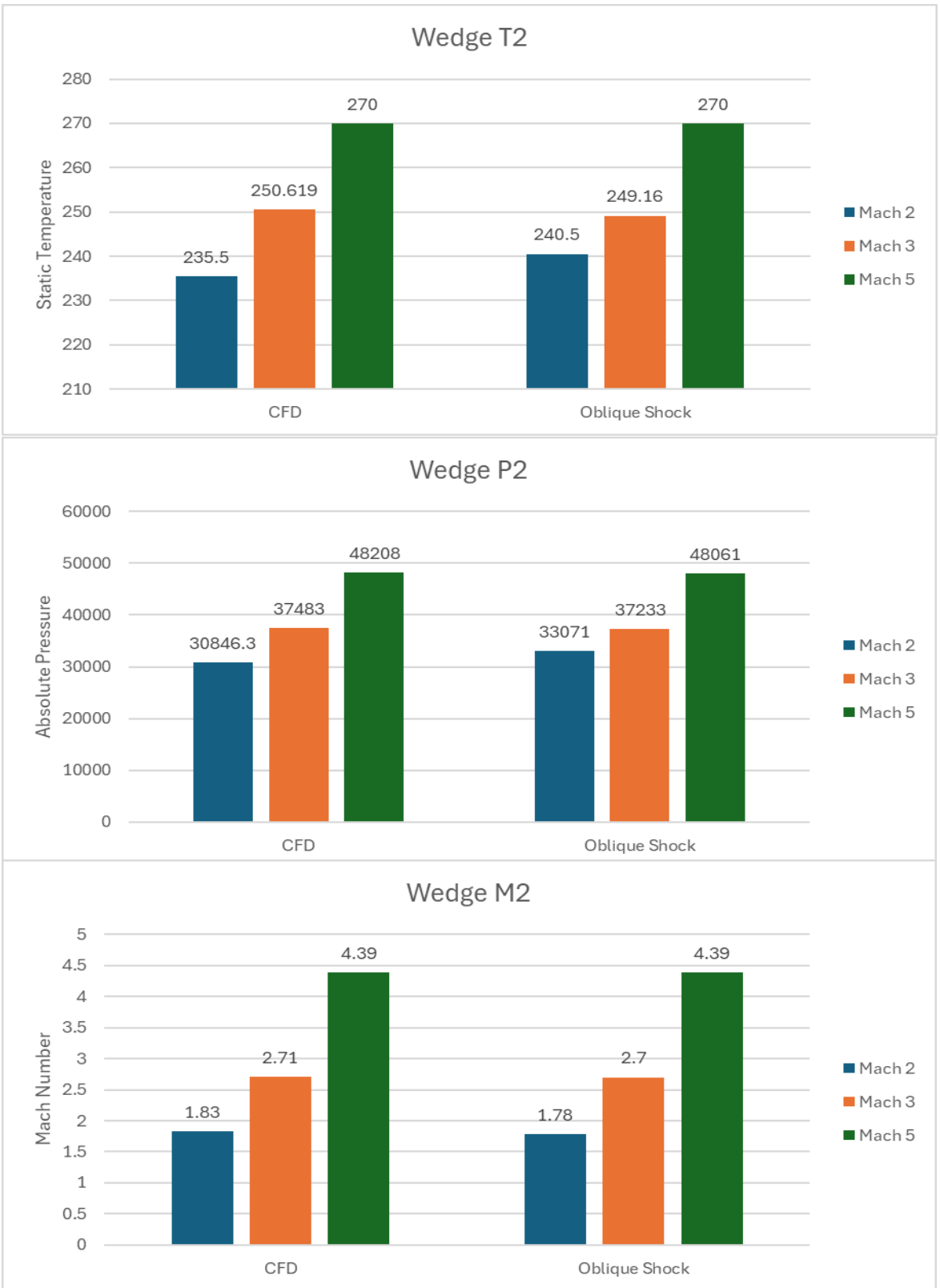

Figure J-2 Wedge Results

K Shock Expansion Theory MATLAB Code

```
clc;
clear;
close;

%Mach Number
m=5;
% angle of geometry
theta=6;
% sweep angle
sweepa=20;
%chord length
c=6;
%thickness
t=0.3;
% gamma
y=1.4;
%Freestream Pressure(N/M)
p1=23842;
%Freestream Density(KG/M^3)
rho1=0.3796;
%Freestream Temperature(K)
t1=218.81;
%angle of attack
aoa=0;
% mach angle
macha=asind(1/m);

% mach after mach cone
mc=m*cosd(sweepa);


% calcluating beta angle for shock
a=sqrt(((m^2-1)^2)-(3*((1+((y-1)/2)*m^2))*((1+((y+1)/2)*m^2)))*(tand(theta)^2));
x=(((m^2-1)^3)-9*(1+((y-1)/2)*m^2)*((1+((y-
1)/2)*m^2)+(((y+1)/4)*m^4))*tand(theta)^2)/a^3;


BStrong=atand(((m^2-1)+(2*a*cos((4*pi*0+acos(x))/3)))/((3*(1+((y-
1)/2)*m^2))*tand(theta)));
BWeak=atand(((m^2-1)+(2*a*cos((4*pi*1+acos(x))/3)))/((3*(1+((y-
1)/2)*m^2))*tand(theta)));

% mach number behind beta shock
mn1=m.*sind(BWeak);
mn2=sqrt((mn1.^2+(2/(y-1))./(((2*y)/(y-1))*(mn1.^2)-1));
m2=mn2./sind(BWeak-theta);

%Rho2
rho2=rho1*(((y+1)*(mn1^2))/((y-1)*(mn1^2)+2));

%P2
p2=p1*(1+((2*y)/(y+1))*((mn1^2)-1));
```

```
%T2
t2=t1*(p2/p1)*(rho1/rho2);
```

L Linear Theory MATLAB Code

```
clc;
clear;
close;

global m;
global mc;
global toverc;
global c;
%Mach Number
m=2;
% sweep angle
sweepa=30;
%chord length
c=6;
%thicknessratio
toverc=0.05;
%Angle of Attack
aoad=0:0.05:6;
aoa = deg2rad(aoad);
%aoa=0;
% mach angle
macha=asind(1/m);


% mach after mach cone
mc=m*cosd(sweepa);
if sweepa>macha
    m=mc;
end

cl=arrayfun(@linearCl,aoa);

cdWedge=arrayfun(@linearWedgeCd,aoa);

cdBiconvex=arrayfun(@linearBiconvexCd,aoa);

% plot(aoad,cl);
% hold on
% plot(aoad,cdBiconvex);
% hold off

%writematrix(cdBiconvex.','cdBinconvex.csv')
writematrix(cl.','cl.csv')

writematrix(cdWedge.','cdWedge.csv')

%plot(aoa,cdWedge);
```

```
function cl = linearCl(aoa)
    global mc;

    cl=(4*aoa)/(sqrt((mc^2)-1));
end

function cdWedge = linearWedgeCd(aoa)
    global mc;
    global toverc;
    global c;
    cdWedge=((2)/(sqrt((mc^2)-1))*((aoa^2)+((toverc)^2)))+(4*(aoa*2))/(sqrt((mc^2)-
1));
end
function cdBiconvex = linearBiconvexCd(aoa)
    global mc;
    global toverc;
    global c;
    cdBiconvex=(((2)/(sqrt((mc^2)-
1)))*((aoa^2)+(1.33*((toverc)^2))))+(4*(aoa^2))/(sqrt((mc^2)-1));
    %cdBiconvex=(((2)/(sqrt((mc^2)-1)))*((aoa^2)+(1.33*((t/c)^2))));
end
```

M NACA Windtunnel Data and CFD results for validation

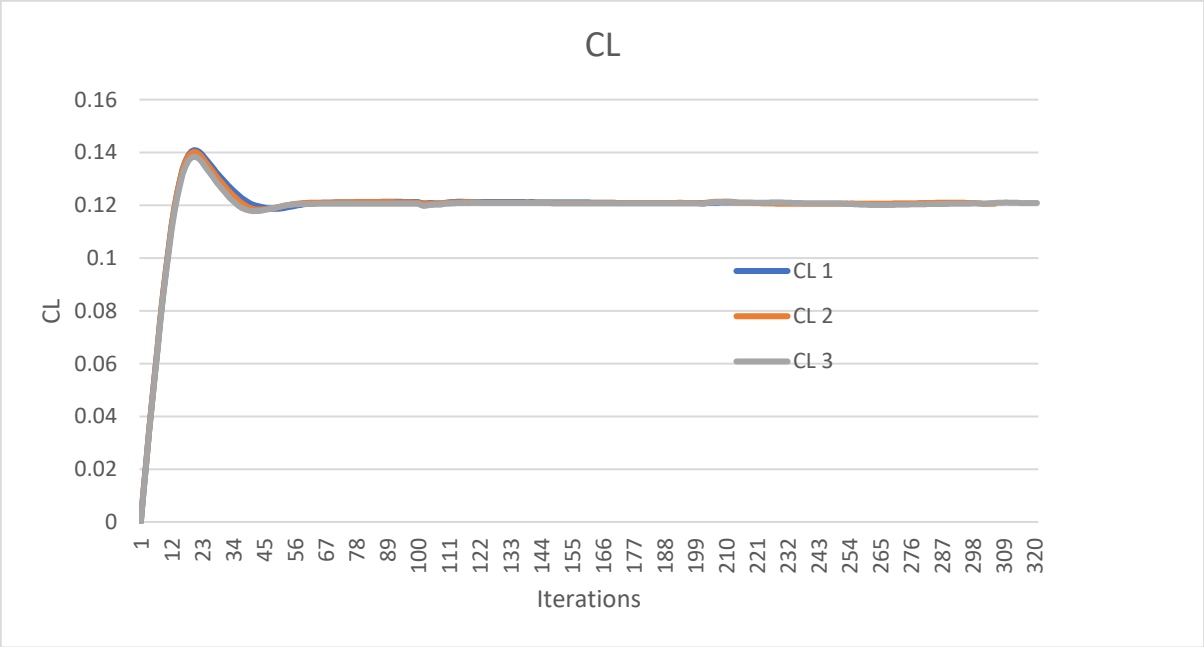

Figure M-1

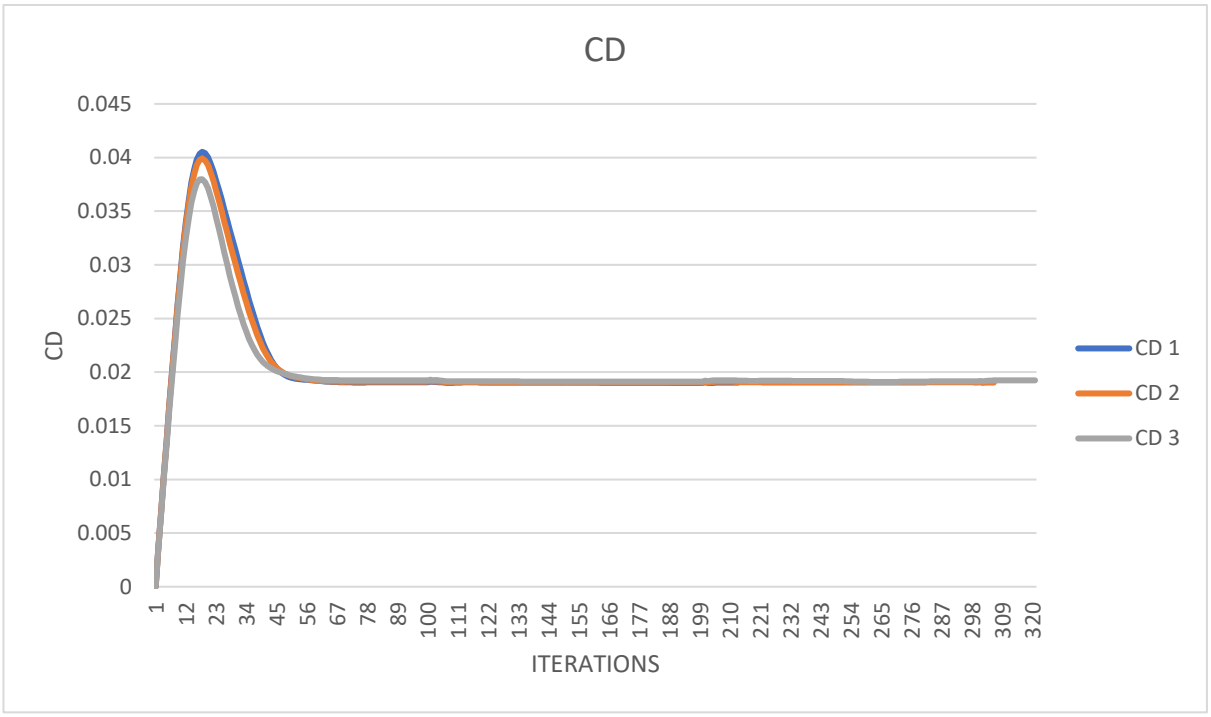

Figure 0-1

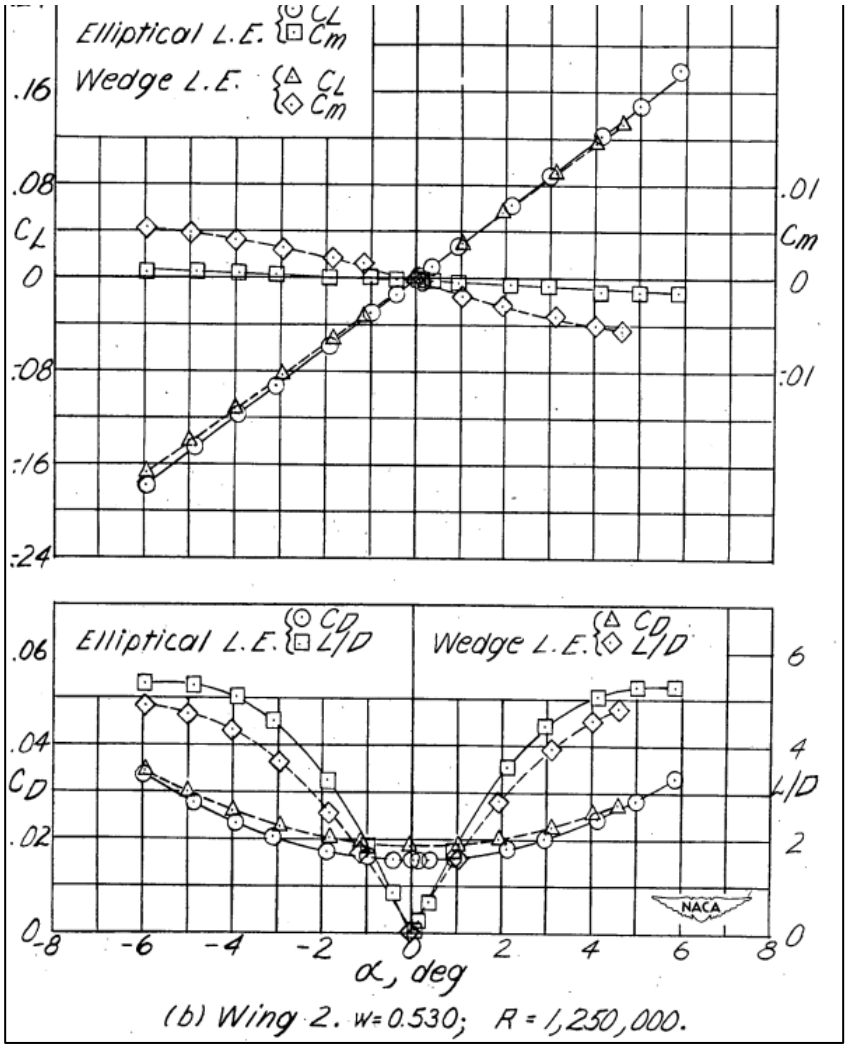

Figure M-3 Results of windtunnel testing(Love 1949)